

## Article

# Origin of Lithium–Potassium-Rich Brines in the Jiangnan Basin, South China: Constraints by Water–Rock Reactions of Mesozoic–Cenozoic Igneous Rocks

Chunlian Wang <sup>1</sup>, Xiaocan Yu <sup>1,\*</sup>, Ruiqin Li <sup>2,3</sup>, Lihong Liu <sup>2,4</sup>, Kai Yan <sup>5</sup> and Chao You <sup>6</sup>

<sup>1</sup> MNR Key Laboratory of Metallogeny and Mineral Assessment, Institute of Mineral Resources, Chinese Academy of Geological Sciences, Beijing 100037, China; wangchunlian312@163.com

<sup>2</sup> School of Earth and Space Sciences, Peking University, Beijing 100871, China; 1601110551@pku.edu.cn (R.L.); liulihong713@163.com (L.L.)

<sup>3</sup> Department of Geological Sciences and Environmental Studies, State University of New York at Binghamton, New York, NY 13902, USA

<sup>4</sup> Oil & Gas Survey, China Geological Survey, Beijing 100083, China

<sup>5</sup> Faculty of Earth Science, University of Iceland, Sturlugata 7, Askja, 101 Reykjavík, Iceland; yankai\_ytq@163.com

<sup>6</sup> Institute of Geological Survey, China University of Geosciences, Wuhan 430074, China; youchao126418@163.com

\* Correspondence: xiaocany1988@163.com



check for updates

**Citation:** Wang, C.; Yu, X.; Li, R.; Liu, L.; Yan, K.; You, C. Origin of Lithium–Potassium-Rich Brines in the Jiangnan Basin, South China: Constraints by Water–Rock Reactions of Mesozoic–Cenozoic Igneous Rocks. *Minerals* **2021**, *11*, 1330. <https://doi.org/10.3390/min11121330>

Academic Editor: Enrique Gomez-Rivas

Received: 12 October 2021

Accepted: 23 November 2021

Published: 28 November 2021

**Publisher's Note:** MDPI stays neutral with regard to jurisdictional claims in published maps and institutional affiliations.



**Copyright:** © 2021 by the authors. Licensee MDPI, Basel, Switzerland. This article is an open access article distributed under the terms and conditions of the Creative Commons Attribution (CC BY) license (<https://creativecommons.org/licenses/by/4.0/>).

**Abstract:** A large number of lithium–potassium-rich brines have been found in Paleocene reservoirs in the Jiangnan Basin, South China. First, the brines have exceptionally high lithium and potassium contents that are even higher than those in other closed basins on the Tibetan Plateau. Second, the enriched brines are widely distributed in the center of the basin. The Mesozoic and Cenozoic igneous rocks in the Jiangling depression are mainly basalt and granite, and their distribution area exceeds 50% of the basin. The large basalt body provided a thermal source for the water–rock reaction. The igneous rocks in the study area could have provided ore-forming elements, such as lithium and potassium, for the brine. A static immersion experiment at room temperature shows that fluids with certain salinities are more likely to activate K ions in basalt. However, weakly alkaline solutions more easily dissolve K. High-temperature water–rock experiments show that the dissolution rates of Ca, Mg, and Sr decrease with increasing temperature, while the dissolution rates of K and Li first increase and then decrease with increasing temperature. The dissolution of K and Li is easier when saline fluid reacts with volcanic rock. The dissolution rate of K is higher than that of Li in basalt, and the dissolution rate of Li is higher than that of K in granite. Compared with the results at normal temperatures, the ability of the fluid to leach elements at higher temperatures is significantly enhanced. Temperature is the main factor controlling the ability of fluid to leach elements. High-salinity fluid is the main carrier of ore-forming elements. According to the water–rock experiments, the mineral composition of the ancient brine in the Jiangling depression that formed during the Paleocene is consistent with that of the ore-rich brine found today, but different by a few orders of magnitude, indicating that the formation of lithium–potassium-rich brines requires a long time. The water–rock reaction is one of the important processes of brine formation, and surface evaporation and concentration are the main mechanisms of brine mineralization.

**Keywords:** Jiangnan Basin; Mesozoic–Cenozoic; water–rock reactions; lithium–potassium-rich brines; mechanisms of brine mineralization

## 1. Introduction

Modern salt lake brines and deep-buried underground brines are often rich in potassium, lithium, boron, rubidium, cesium, and other high-value strategic emerging mineral resources [1–14], and are important raw material sources of potash and lithium globally.

China's external potash dependence has decreased from 75% to 45%, but the consumption has been growing rapidly, from 3.999 million tons in 2000 to 10.19 million tons in 2018, which accounts for approximately 20–25% of the global potash consumption [15]. At present, the potash resource in China is mainly found in the brines of Qaidam, Lop Nur, and other salt lakes in Northwest China. Researchers have predicted that the service life of these resources is about 20 years [16]. China's existing lithium supply is highly dependent on external resources; 70% of the lithium supply was imported in 2017. The lithium ore in China is dominated by the hard rock-type. Lithium brine-type deposits are mainly distributed in the western plateau area and are greatly restricted by mining conditions and technology due to their high Mg/Li ratios. The world's large and super-large lithium deposits are mainly brine-type, accounting for 75% of the global lithium production, which is mainly from salt lake lithium-rich brine in South America, the western plateau of North America, and lithium-rich underground hot water in New Zealand [17]. These lithium-rich brines or underground hot water reservoirs all have very low Mg/Li ratios and are easy to extract. The common characteristics of these regions are that they are all located in active tectonic regions with dry climates, making them conducive to material concentration and mineralization. When the Pacific Plate subducted under the Eurasian plate, and the Indian Plate converged and collided with the Eurasian Plate, the two processes were alternately active, resulting in a strong stress release zone in the eastern part of China that has been present since the Jurassic; this has formed a giant rift system in eastern China. The Jianghan Basin is located in this rift system, which has structural conditions that are conducive for the formation of large-scale lithium brine deposits, similar to those found abroad.

The research developments regarding the source and genesis of potassium and lithium in the brine have been introduced in depth. Lowenstein et al. (1989) [18] proposed that some abnormal potassium salts may be formed in nonmarine brine rather than seawater, indicating that their provenance is richer in potassium ions than seawater, and there are abnormal replenishing sources. Holmearda and Hutchinsan (1968) [19] proposed that potassium was formed by rift thermal halogen, as in the case of the Ethiopian salt lake (belonging to the Red Sea rift system) distributed near Black Mountain and Round Mountain in the middle part of the Danakil Depression, which was formed by some brine pools formed by a thermal halogen spring rising from underground, accompanied by the precipitation of many potassium salts and other salts. The hot brine spring in Black Mountain is composed of high-temperature (up to 130 °C) saturated brine with a potassium chloride content of about 2%. In Katwe crater lake, an East African Rift salt lake on the Uganda border, the area of volcanic rock is mainly basic rock with a high K/Na ratio; more than 50 springs supply the lake; and potassium content of the lake is 2.2–45 g/L, bromine content is 0.5–2.55 g/L, and fluorine content is 0.1–0.5 g/L [20].

Lithium deposits in salt lake brine are associated with potassium salt and also go through the evaporation enrichment process. Yu et al. (2021) [21] proposed a preliminary model and pointed out that the lithium mineralization of brine is mainly by evaporation and the reaction between hot fluid and aquifer. Godfrey et al. (2013) [2] proposed that climate plays an important influence on lithium enrichment in salt lake brine; that is, the high-altitude drought in the middle Andes leads to rapid enrichment of lithium in brine. Munk et al. (2018) [11] summarized the metallogenic characteristics of 18 lithium brine deposits in the world. Munk and Chamberlain (2011) [22] proposed that the genesis model of lithium-rich brines in Clayton Valley, Nevada, is as follows: (1) lithium coming from the leaching of lithium-rich rhyolite; (2) condensing and evaporating in dry salt lakes; and (3) the underground mixing of brine and the evolution of water–rock reaction. Hofstra et al. (2013) [23] summarized and proposed the formation mode of lithium-rich brine deposit and lithium clay ore in Clayton Valley Salt Lake in the United States, namely partial remelting of A-type or S-type granite (up-invasion, eruption) and lithium filtering into the salt lake from the forest, finally forming lithium-rich brine deposits by processes such as evaporation and concentration. The formation of lithium-rich brines in Puna Salt Lakes in Argentina is related to the contribution of hot water and weathering of lithium-bearing rocks [24].

Price et al. (2000) [25] believed that lithium-rich brine in Clayton Valley Salt Lake, Nevada, western United States, may come from the weathering products of lithium-rich volcanic ash or rhyolite; Araoka et al. (2013) [26] believed that lithium-rich intercrystalline brine of the dry salt lake in Nevada, United States, mainly came from high-temperature water–rock (volcanic rock) reaction and local hot spring activities, rather than from low-temperature weathering products of surface materials.

One common feature of lithium–potassium-rich brines mentioned is the development of volcanic activity in the basin. Active and dormant volcanoes plus the massive magmatic body are important as heat sources, which enhance water–rock reactions [14,17,25].

The concentrations of KCl and LiCl in the brine in the Jiangling depression reach 1.64% and 300–800 mg/L, respectively, both of which have met the formal and official requirements of industrial development in China. The brine is a liquid-type potassium- and lithium-rich deposit and has a high comprehensive utilization value [5,27,28]. Therefore, it is of great significance to study the source and enrichment process of mineralization in the brine to establish a metallogenic model of potassium- and lithium-rich brine and guide the further prospecting of potassium- and lithium-rich brine in this area. Magmatic activity in Middle Cenozoic was frequent in and around the basin. Basalt and granite are rich in potassium, lithium, rubidium, tungsten, tin, and other elements [29–31], which may have been the main source of minerals for the deep-buried brine in the basin. Whether the ore-forming materials of potassium–lithium-rich brine were directly enriched by water–rock reactions or formed by surface weathering, evaporation, and concentration and finally sealed storage is the subject of this research. To solve the scientific problem of the material source and enrichment process of potassium and lithium in the brine in the Jiangling depression, potassium–lithium-rich brine and Cenozoic igneous rocks around the Jiangling depression were selected for analysis of the chemical constituents of brine and rocks. The water–rock reaction process of basalt and granite was carried out by using a reaction kettle to explore its significance to the material source and genesis of the potassium–lithium-rich brine.

## 2. Geological Background

The Jiangnan Basin, which covers an area of almost 36,360 km<sup>2</sup>, is located in Hubei Province in South China (Figure 1A). It is one of a series of northeast–southwest-oriented Mesozoic–Cenozoic continental rift basins in East Asia [32–34]. It formed in a back-arc extensional tectonic setting due to widespread regional extensional subsidence caused by the eastward rollback of the subducting Pacific Plate that has occurred since the Mesozoic [35–37]. The Jiangnan Basin is bounded by NNE-trending normal faults and is underlain by the crystalline basement of the Yangtze Craton [38,39]. It is located between two Mesozoic orogenic belts: the Qinling–Dabie orogenic belt to the north and the Xuefeng orogenic belt to the south. It is also bordered to the west by the Huangling Dome along the Three Gorges of the Yangtze River [39] and to the southwest by the Yidu–Hefeng Anticline (Figure 1B).

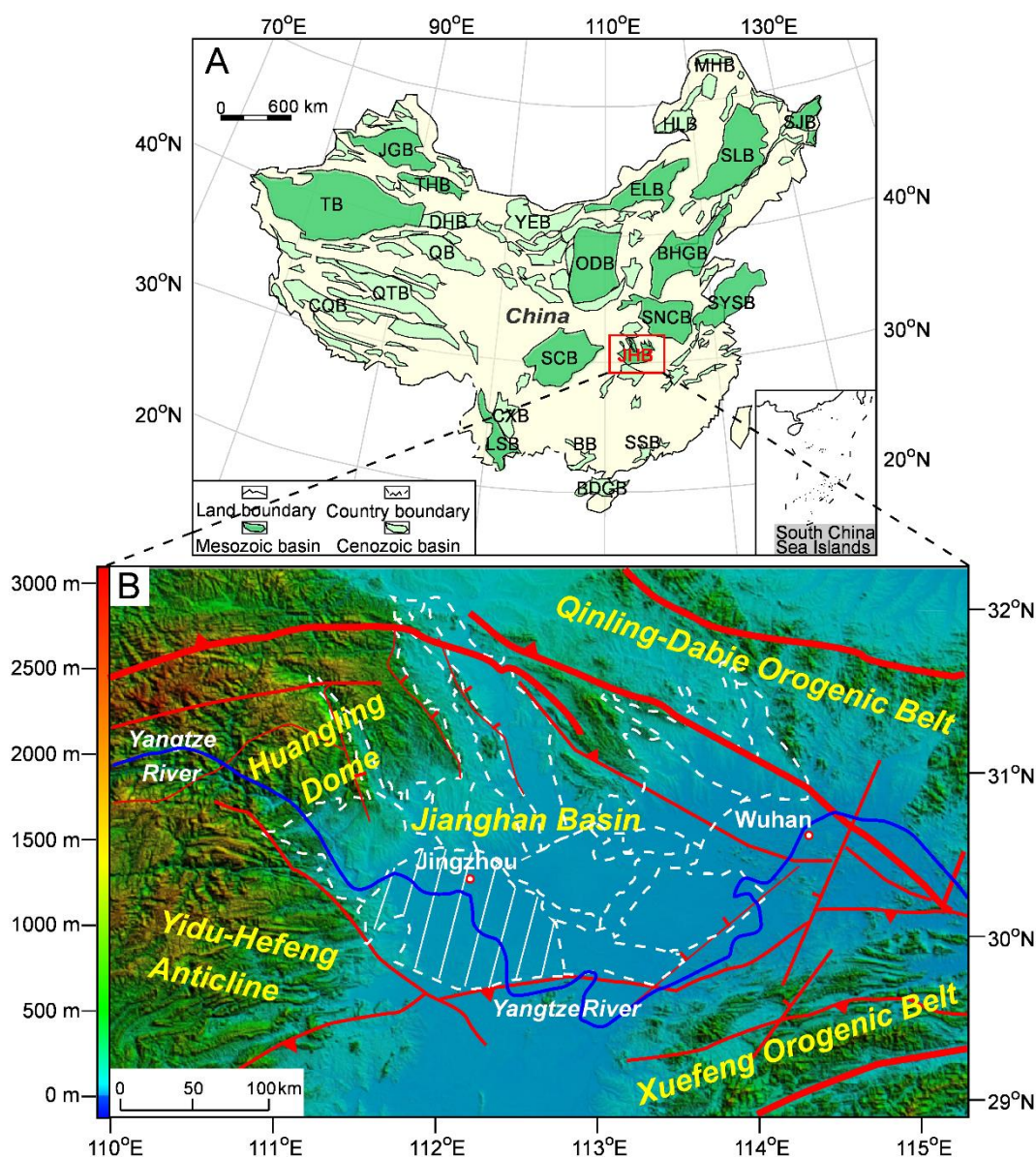


**Figure 1.** (A) Distribution of major Mesozoic–Cenozoic basins in China and location of Jiangnan basin. BB, Baise Basin; BGB, Baidu Gulf Basin; BHG, Bohai Gulf Basin; CQB, Cuoqing Basin; CXB, Chuxiong Basin; DHB, Dunhuang Basin; ELB, Erlian Basin; HLB, Hailaer Basin; JGB, Junggar Basin; JHB, Jiangnan Basin; LSB, Lanping–Simao Basin; MHB, Mehe Basin; ODB, Ordos Basin; QB, Qaidam Basin; QTB, Qiangtang Basin; SCB, Sichuan Basin; SJB, Sanjiang Basin; SLB, Songliao Basin; SNCB, Southern North China Basin; SSB, Sanshui Basin; SYSB, South Yellow Sea Basin; TB, Tarim Basin; THB, Turpan–Hami Basin; YEB, Yingen–Ejinaqi Basin. (B) DEM map showing the location of the Jiangling depression (diagonal white solid lines) in the Jiangnan Basin (white dashed lines). The red lines show the major faults surrounding the basin. Geological data from [40].

The Jiangnan Basin is surrounded by high mountains that are 1000–3000 m above sea level. Its periphery is surrounded by low hills with a height of more than 120 m, and the central area is a large plains area [41]. The interior of the basin is covered by Quaternary sediments, and the lower strata are exposed only at the edge of the basin (Figure 2A). The Yangtze River flows from the northwest to the southeast and then to the northeast (Figure 2B). There is hot-spring activity in the Songzi area of the basin. The Jiangnan Basin is composed of Neoproterozoic to Middle Triassic marine carbonate rocks and continental shelf clastic rocks, Late Triassic to Early Cretaceous continental clastic rocks, and a large number of Late Cretaceous to Paleocene evaporite rocks and a clastic rock series interbedded with basalt (Figure 2C).



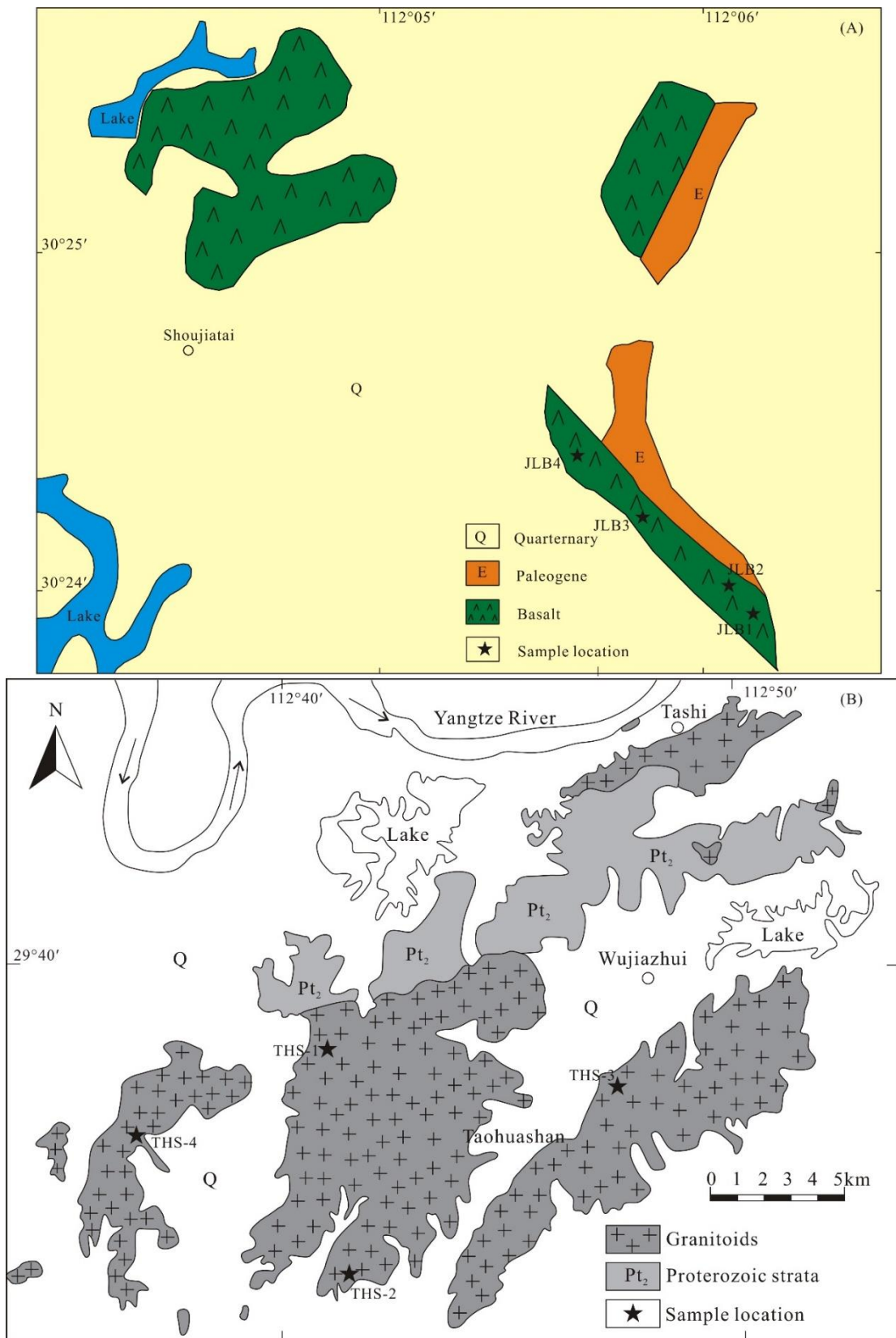


**Figure 3.** Geological sketch map of the Balingshan basalt (A) and the Taohuashan granitoids (B) and sample location (modified from [9]).

### 3. Samples and Methods

Six brine samples were collected from two boreholes (wells GJ1 and SJ4) for this study. Samples N1-1, N1-2, and N1-3 were collected from well GJ1. Samples S1-1, S1-2, and S1-3 were collected from well SJ4. The brine from well GJ1 was collected from the Paleocene fractured mudstone reservoir at a depth of 3571 m. The brine from well SJ4 was collected from the basalt pore-type reservoir at a depth of 3880 m (Figure 2B). Four basalt samples were collected from a field outcrop in the Balingshan area in the northern Jiangling depression (Figure 3A). Four granite samples were collected from a field outcrop in the Taohuashan area in the southeast of the depression (Figure 3B).

The composition analysis of the potassium–lithium-rich brine and major elements was completed by the National Geological Testing Center, in which Cl and SO<sub>4</sub> were tested by the titration method of AgNO<sub>3</sub> and BaCl<sub>2</sub>, and the analysis error was less than 3%. The other main elements were tested by inductively coupled plasma optical emission spectroscopy (ICP-OES), and the analysis error was less than 5%. Trace elements were determined by plasma mass spectrometry (X-series).

Through the microscopic identification of thin sections, petrography of the igneous rock was studied to determine the mineral assemblage, composition, structure, alteration characteristics of the surrounding rock, rock type, and inclusions in the rock.

Some fresh granite and basalt samples were selected and crushed to 200 mesh and sent to the National Geological Experiment and Test Center of the Ministry of Natural and Resources for major and trace element analyses. The major elements were detected by fused X-ray fluorescence spectrometry (XRF-PW4400) based on GB/T14506.28-2010, and the analysis error was less than 2–5%. Trace elements were detected by plasma mass spectrometer (ICPMS-PE300D) based on GB/T14506.30-2010, and the analysis error was less than 5–10%.

The appropriate granite and basalt samples were selected, the weathered and attached objects on the surface of the samples were removed, and the samples were coarsely crushed. After cleaning and drying, the samples were finely crushed to a size of 60~80 mesh with a crushing machine, from which 20 g samples were sifted. Attention was given to ensure that the samples were clean and not contaminated. Water–rock reaction experiments were carried out in the laboratory with a reactor device at different temperatures, reaction times, fluid compositions, and fluid types, and the reaction products were measured by inductively coupled plasma atomic emission spectrometry (ICP-AES). The experiment of the water-rock reaction due to static immersion of igneous rock was carried out under normal temperature and pressure conditions. The reaction fluid conditions were distilled water, 1 mol/L NaCl, 2 mol/L NaCl, pH = 5, and pH = 8, and the sampling times were on the 1st, 5th, 11th, 19th, 29th, 41st, and 55th days. To explore the influence of reaction time on the dissolved elements, one granite sample and one basalt sample were selected for this experiment. The reaction solution was a 1 mol/L NaCl solution, the total reaction time was 6 h, the reaction temperature was 150 °C, the average sampling time was once per hour, and the two samples were sampled 12 times in total. To explore the effect of reaction temperature and fluid composition on the element dissolution amount, one basalt sample and one granite sample were selected; the reaction time was 4 h; the reaction temperatures were 200, 250, 300, 350, and 400 °C; the reaction fluid was distilled water and 1 mol/L NaCl solution; and each sample was sampled 10 times for a total of 20 times.

## 4. Results

### 4.1. Brine Composition

According to the observations from two boreholes (GJ1 and SJ4), the brine deposits are distributed from 1500 m to 5000 m underground in the basin. Brine occurs in tectonic fracture zones, sandstone pores, and basalt fractures of the Paleocene Shashi and Xin'gouzui formations [9]. Brine is pressure-bearing. The results of large-scale pumping experiments show that the water flow in multiple wells is stable, and the water inflow in each well is more than 1000 m<sup>3</sup>/d. The lithium and potassium content in the deep-buried brine reaches

industrial grade, and it also contains other beneficial components such as B and Br (Table 1). The contents of sodium, chloride, potassium, calcium, sulfate, lithium, boron, and strontium are 102.97–113.93 g/L, 182.68–202.02 g/L, 6.32–10.35 g/L, 4.16–13.56 g/L, 0.24–0.54 g/L, 44.15–107.41 mg/L, 588.23–971.99 mg/L, and 402.02–1031.70 mg/L, respectively (Table 1).

**Table 1.** Chemical composition of lithium–potassium-rich brines in Jiangling depression. Samples N1 and S1 are from wells GJ1 and SJ4, respectively.

Sample	TDS (g/L)	pH	K (g/L)	Na (g/L)	Ca (g/L)	Mg (g/L)	Cl (g/L)	SO <sub>4</sub> (g/L)	B (mg/L)	Li (mg/L)	Sr (mg/L)	Br (mg/L)	I (mg/L)
N1-1	331	5.90	10.18	111.87	4.16	0.22	183.48	0.41	950.66	104.71	409.73	461.92	31.91
N1-2	335	5.93	10.26	113.93	4.23	0.21	184.59	0.32	971.99	105.58	406.38	440.30	31.75
N1-3	332	5.99	10.35	112.82	4.35	0.22	182.68	0.54	960.62	107.41	402.02	433.02	31.95
S1-1	359	6.52	6.99	106.10	13.56	0.04	202.02	0.26	588.23	48.61	1031.70	227.60	39.05
S1-2	352	6.58	6.41	105.20	12.46	0.05	197.70	0.24	651.40	44.25	955.85	206.65	36.15
S1-3	351	6.50	6.32	102.97	12.37	0.06	194.42	0.28	642.18	44.15	954.50	203.30	35.65

The SiO<sub>2</sub> content in the basalt ranges from 48.03% to 52.55%, with an average value of 50.92%. The Na<sub>2</sub>O content varies from 3.85% to 5.56%, with an average of 4.79%. The K<sub>2</sub>O content varies from 0.36% to 2.05%, with an average of 1.00%; the Al<sub>2</sub>O<sub>3</sub> content varies from 12.30% to 14.00%, with an average of 13.45%; and the CaO content varies from 4.23% to 7.35%, with an average of 5.76%.

## 4.2. Petrology and Mineralogy

### 4.2.1. Basalt

Basalt is the most widely distributed volcanic rock in the Jiangling depression. Longitudinally, it is characterized by the alternating occurrence of red stomatal nodular basalt and dark grey dense massive basalt (Figures 4A and 5B). The pores of the red stomatal nodular basalt are filled with minerals such as zeolite, chlorite, calcite, and opal (Figure 4A). The dark grey-green dense massive basalt has columnar joints (Figure 4C), in which the calcite and quartz veins are extremely well developed, ranging from 1 to 5 cm in width, most often up to several meters (Figure 4D). Microscopic observation shows that the basalt has an obvious intergranular structure, and olivine alteration is strong, resulting in chloritization and iddingsitization (Figure 4E). Plagioclase and pyroxene are the main weakly altered rock-forming minerals (Figure 4F), and the accessory minerals are mainly magnetite, ilmenite, apatite, etc.

According to the major element analysis of basalt samples in the Jiangling depression (Table 2), the SiO<sub>2</sub> content in the basalt ranges from 52.86% to 53.10%, with an average value of 52.99%. The Na<sub>2</sub>O content varies from 3.24% to 3.87%, with an average of 3.48%. The K<sub>2</sub>O content varies from 1.03% to 1.20%, with an average of 1.09%. The Al<sub>2</sub>O<sub>3</sub> content ranges from 13.03% to 14.00%, with an average of 13.54%. The CaO content ranges from 6.23% to 8.55%, with an average of 7.34%.

**Table 2.** Main elements of basalt in Jiangling depression (%). The last four samples are from [47].

Samples	SiO <sub>2</sub>	TiO <sub>2</sub>	Al <sub>2</sub> O <sub>3</sub>	TFe <sub>2</sub> O <sub>3</sub>	MnO	MgO	CaO	Na <sub>2</sub> O	K <sub>2</sub> O	P <sub>2</sub> O <sub>5</sub>	LOI	Li (µg/g)	Zr (µg/g)	Total
JLB1	53.04	2.00	14.00	9.24	0.18	8.32	6.37	3.25	1.03	0.20	1.89	15.0	147	99.82
JLB2	53.10	1.95	13.03	9.64	0.10	8.29	6.23	3.24	1.20	0.22	1.85	29.6	152	99.95
JLB3	52.94	2.03	13.25	8.98	0.10	7.49	8.55	3.56	1.05	0.22	1.63	17.9	159	99.81
JLB4	52.86	2.26	13.86	8.82	0.17	6.82	8.21	3.87	1.09	0.29	1.63	19.0	149	100.09
18DT10	49.77	2.28	14.77	12.65	0.15	7.29	8.84	3.08	0.82	0.37	0	7.26	158	100.02
18DT12	51.68	1.99	14.01	12.33	0.16	7.34	8.05	3.21	0.63	0.26	0	5.43	136	99.66
18DT13	53.45	1.82	14.14	11.95	0.16	6.71	7.83	3.28	0.75	0.21	0	5.34	124	100.28
18DT14	52.28	1.89	14.03	12.23	0.16	7.18	8.03	3.09	0.49	0.21	0	4.87	128	99.58



**Figure 4.** Field outcrops and microscopic photographs of basalt in Jiangling depression. (A) Red stomata almond-shaped basalt; (B) dense massive basalt; (C) columnar jointed basalt; (D) calcite and quartz veins developed in basalt; (E) intergranular basalt. Olivine undergoes intense alteration, chloritization, and iddingsitization; perpendicular polarized light. Plagioclase is colorless and transparent and has two groups of complete cleavage; long strip, polarization microscope common twin, interference color level gray, negative low protrusion. (F) Basalt is mainly composed of plagioclase (Pl) and pyroxene (Px), with weak alteration pairs; perpendicular polarized light. Pyroxene is the most common mineral in ultrabasic rocks and mafic rocks. It is greenish black and has two groups of nearly vertical cleavage, often forming irregular stepped fractures.

#### 4.2.2. Granite

The analysis results of the major element composition of granite around the Jiangling depression (Table 3) reveal that the  $\text{SiO}_2$  content in granite is high, ranging from 70.33% to 73.05%, with an average of 71.37%; the content of  $\text{K}_2\text{O}$  varies from 4.64% to 5.35%, with an average of 5.04%; the content of  $\text{Na}_2\text{O}$  varies from 2.88% to 3.62%, with an average of 3.20%; the content of  $\text{Al}_2\text{O}_3$  varies from 14.10% to 15.14%, with an average of 14.68%; and the content of  $\text{CaO}$  ranges from 1.26% to 2.04%, with an average of 1.76%.

**Table 3.** Main elements of Cretaceous granite in Jiangling depression (%). The last five samples are from [48].

Samples	SiO <sub>2</sub>	TiO <sub>2</sub>	Al <sub>2</sub> O <sub>3</sub>	TFe <sub>2</sub> O <sub>3</sub>	MnO	MgO	CaO	Na <sub>2</sub> O	K <sub>2</sub> O	P <sub>2</sub> O <sub>5</sub>	LOI	Li (µg/g)	Total
THS-1	73.05	0.15	14.10	1.50	0.04	0.30	1.26	3.62	5.35	0.08	0.48	90.6	100.12
THS-2	70.33	0.35	15.14	2.23	0.04	0.63	2.04	2.88	4.64	0.13	1.06	82.0	99.85
THS-3	71.30	0.17	14.39	1.89	0.04	0.48	1.88	3.17	5.19	0.11	0.89	102.0	99.78
THS-4	70.78	0.36	15.10	1.96	0.05	0.51	1.84	3.12	4.96	0.09	0.77	82.0	99.82
KKTH117	73.45	0.18	14.22	1.74	0.06	0.37	2.05	3.29	3.26	0.04	0.63	72	99.93
KKTH118	72.96	0.23	14.24	2.16	0.05	0.52	2.33	3.11	3.13	0.05	0.64	82	100.14
KKTH119	70.69	0.18	15.74	1.68	0.04	0.35	2.13	3.06	4.94	0.05	0.53	80.8	99.87
KKTH120	72.30	0.19	14.96	1.86	0.05	0.42	2.21	3.06	3.91	0.07	0.80	67.6	100.46
KKTH121	73.81	0.21	14.00	2.15	0.05	0.49	2.43	3.36	2.62	0.06	0.60	83.1	100.24

#### 4.3. Experiment Results of the Water–Rock Reaction Due to Basalt Static Immersion

The experimental results of the water–rock reaction due to static immersion are shown in Table 4.

**Table 4.** Results of basalt static immersion experiment.

Samples	Lithology	Fluid	Time (Days)	Ion Concentration (mg·L <sup>-1</sup> )						
				K	Ca	Mg	Sr	B	Br	I
JLB1	Basalt	Distilled water	1	1.1	5.63	0.55	0.04	-	-	-
JLB1	Basalt	Distilled water	5	1.12	8.62	0.79	0.05	-	-	-
JLB1	Basalt	Distilled water	11	1.56	11.58	1.29	0.06	-	-	-
JLB1	Basalt	Distilled water	19	2.28	14.80	1.59	0.07	-	-	-
JLB1	Basalt	Distilled water	29	2.88	17.82	1.98	0.08	-	-	-
JLB1	Basalt	Distilled water	41	3.82	19.99	2.21	0.09	-	-	-
JLB1	Basalt	Distilled water	55	5.12	21.92	2.65	0.11	-	-	-
JLB1	Basalt	1 mol/L NaCl	1	3.06	226.91	12.40	1.25	0.07	3.23	0.16
JLB1	Basalt	1 mol/L NaCl	5	3.15	245.69	13.95	1.33	0.07	3.48	0.15
JLB1	Basalt	1 mol/L NaCl	11	3.28	259.68	14.41	1.39	0.07	3.46	0.16
JLB1	Basalt	1 mol/L NaCl	19	3.36	275.64	14.82	1.34	0.07	3.39	0.14
JLB1	Basalt	1 mol/L NaCl	29	4.40	279.88	14.65	1.41	0.08	3.16	0.16
JLB1	Basalt	1 mol/L NaCl	41	7.97	288.28	18.66	1.52	0.08	3.98	-
JLB1	Basalt	1 mol/L NaCl	55	10.90	299.40	18.97	1.59	0.08	4.87	-
JLB1	Basalt	2 mol/L NaCl	1	6.77	272.96	18.87	1.55	0.25	8.45	0.45
JLB1	Basalt	2 mol/L NaCl	5	6.98	301.85	20.35	1.68	0.28	7.99	0.41
JLB1	Basalt	2 mol/L NaCl	11	7.42	321.52	20.81	1.72	0.26	8.68	0.43
JLB1	Basalt	2 mol/L NaCl	19	8.51	322.65	20.95	1.74	0.25	7.55	0.19
JLB1	Basalt	2 mol/L NaCl	29	8.98	324.84	20.54	1.73	0.32	8.52	0.35
JLB1	Basalt	2 mol/L NaCl	41	11.93	328.15	21.58	1.78	0.28	10.28	-
JLB1	Basalt	2 mol/L NaCl	55	14.86	343.45	22.79	1.90	0.28	10.13	-
JLB1	Basalt	Ph = 5	1	0.31	22.51	4.03	0.12	-	-	-
JLB1	Basalt	Ph = 5	5	0.42	36.98	7.10	0.19	-	-	-
JLB1	Basalt	Ph = 5	11	0.43	39.05	7.96	0.19	-	-	-
JLB1	Basalt	Ph = 5	19	0.42	38.54	8.45	0.20	-	-	-
JLB1	Basalt	Ph = 5	29	0.44	40.72	8.91	0.21	-	-	-
JLB1	Basalt	Ph = 5	41	0	38.64	9.35	0.20	-	-	-
JLB1	Basalt	Ph = 5	55	10.44	40.69	10.08	0.20	-	-	-
JLB1	Basalt	Ph = 8	1	0	0.24	0.31	0	-	-	-
JLB1	Basalt	Ph = 8	5	16.96	0.79	0.44	0	-	-	-
JLB1	Basalt	Ph = 8	11	10.55	1.28	0.56	0	-	-	-
JLB1	Basalt	Ph = 8	19	12.42	1.73	0.69	0.01	-	-	-
JLB1	Basalt	Ph = 8	29	26.81	1.99	0.88	0.01	-	-	-
JLB1	Basalt	Ph = 8	41	0	2.38	0.96	0.01	-	-	-
JLB1	Basalt	Ph = 8	55	3.57	2.93	1.18	0.01	-	-	-

Table 4. Cont.

Samples	Lithology	Fluid	Time (Days)	Ion Concentration (mg·L <sup>-1</sup> )						
				K	Ca	Mg	Sr	B	Br	I
THS-1	Granite	Distilled water	1	0.42	0.56	0.04	0.01	-	-	-
THS-1	Granite	Distilled water	5	0.52	0.93	0.06	0.01	-	-	-
THS-1	Granite	Distilled water	11	0.64	1.65	0.11	0.02	-	-	-
THS-1	Granite	Distilled water	19	0.83	1.98	0.13	0.02	-	-	-
THS-1	Granite	Distilled water	29	0.74	2.77	0.15	0.03	-	-	-
THS-1	Granite	Distilled water	41	0.91	3.29	0.23	0.03	-	-	-
THS-1	Granite	Distilled water	55	1.49	4.11	0.26	0.04	-	-	-
THS-1	Granite	1 mol/L NaCl	1	0.88	18.33	0.69	0.07	0.03	2.22	0.10
THS-1	Granite	1 mol/L NaCl	5	0.9	21.48	0.78	0.08	0.03	2.19	0.11
THS-1	Granite	1 mol/L NaCl	11	0.95	22.69	0.78	0.08	0.04	2.25	0.10
THS-1	Granite	1 mol/L NaCl	19	1.02	23.94	0.81	0.08	0.03	2.15	0.11
THS-1	Granite	1 mol/L NaCl	29	1.03	24.49	0.84	0.08	0.04	3.14	0.11
THS-1	Granite	1 mol/L NaCl	41	1.08	27.06	1.11	0.09	0.04	3.13	-
THS-1	Granite	1 mol/L NaCl	55	1.18	27.87	1.15	0.10	0.04	3.16	-
THS-1	Granite	2 mol/L NaCl	1	2.18	22.66	1.01	0.09	0.12	5.32	0.20
THS-1	Granite	2 mol/L NaCl	5	2.26	26.68	1.06	0.09	0.15	5.65	0.27
THS-1	Granite	2 mol/L NaCl	11	2.4	27.67	1.08	0.09	0.16	5.22	0.31
THS-1	Granite	2 mol/L NaCl	19	2.66	28.99	1.13	0.10	0.18	4.96	0.32
THS-1	Granite	2 mol/L NaCl	29	2.88	30.14	1.14	0.10	0.11	5.86	0.28
THS-1	Granite	2 mol/L NaCl	41	3.15	30.85	1.22	0.11	0.13	7.23	-
THS-1	Granite	2 mol/L NaCl	55	5.29	30.67	1.22	0.11	0.13	7.44	-
THS-1	Granite	Ph = 5	1	0.07	4.55	0.24	0.12	-	-	-
THS-1	Granite	Ph = 5	5	0.09	5.89	0.36	0.15	-	-	-
THS-1	Granite	Ph = 5	11	0.09	6.63	0.51	0.18	-	-	-
THS-1	Granite	Ph = 5	19	0.09	6.85	0.63	0.21	-	-	-
THS-1	Granite	Ph = 5	29	0.07	7.46	0.75	0.22	-	-	-
THS-1	Granite	Ph = 5	41	3.19	7.64	1.23	0.27	-	-	-
THS-1	Granite	Ph = 5	55	-	8.06	1.26	0.34	-	-	-
THS-1	Granite	Ph = 8	1	2.34	0.63	0.02	0	-	-	-
THS-1	Granite	Ph = 8	5	3.14	1.47	0.11	0	-	-	-
THS-1	Granite	Ph = 8	11	3.20	1.60	0.15	0.01	-	-	-
THS-1	Granite	Ph = 8	19	2.12	2.81	0.21	0.01	-	-	-
THS-1	Granite	Ph = 8	29	4.23	3.13	0.30	0.01	-	-	-
THS-1	Granite	Ph = 8	41	6.83	4.20	0.37	0.01	-	-	-
THS-1	Granite	Ph = 8	55	-	5.42	0.43	0.02	-	-	-

Note: - means below the detection limit.

#### 4.4. Results of High-Temperature Water–Rock Reactions

##### 4.4.1. Experiment of Water–Rock Reactions over Time

The experimental results of water–rock reactions over time are shown in Table 5.

Table 5. The water–rock reaction experiment results with variable time.

Samples	Lithology	Fluid (NaCl)	T (°C)	Time (h)	Ion Concentration (mg/L)						
					K	Li	Mg	Sr	Ca	S	Br
JLB1	Basalt	1 mol/L	150	1	28.59	0.03	102.3	0.52	7.99	1.61	0.31
JLB1	Basalt	1 mol/L	150	2	25.98	0.01	117.57	1.67	7.74	1.51	0.21
JLB1	Basalt	1 mol/L	150	3	33.50	0.05	73.11	0.51	9.97	1.92	0.22
JLB1	Basalt	1 mol/L	150	4	19.66	0.03	125.52	0.68	6.42	1.23	0.55
JLB1	Basalt	1 mol/L	150	5	27.04	0.02	89.52	0.40	9.32	1.91	0.61
JLB1	Basalt	1 mol/L	150	6	22.13	0.01	124.28	0.57	6.85	1.87	0.60
THS-1	Granite	1 mol/L	150	1	9.76	0.04	39.37	0.07	0.28	0.67	0.49
THS-1	Granite	1 mol/L	150	2	8.05	0.05	28.47	0.06	0.62	0.58	0.47
THS-1	Granite	1 mol/L	150	3	11.32	0.06	35.51	0.05	0.84	0.69	0.41
THS-1	Granite	1 mol/L	150	4	14.21	0.09	38.04	0.03	0.39	0.66	0.43
THS-1	Granite	1 mol/L	150	5	16.68	0.05	44.27	0.04	0.46	0.96	0.63
THS-1	Granite	1 mol/L	150	6	3.87	0.02	21.66	0.03	0.25	0.86	0.49

#### 4.4.2. Experiment of Water–Rock Reactions with Variable Temperatures

The experimental results of water–rock reactions with variable temperature are shown in Table 6.

**Table 6.** The water–rock reaction experiment results with variable temperature.

Samples	Lithology	Fluid/Solution	T (°C)	Ion Concentration (mg/L)					
				K	Ca	Mg	Sr	Li	Br
JLB1	Basalt	Distilled water	200	2.423	17.047	1.300	-	0.005	0.184
JLB1	Basalt	Distilled water	250	6.424	13.181	0.541	-	0.014	0.197
JLB1	Basalt	Distilled water	300	4.172	1.136	0.172	-	0.013	-
JLB1	Basalt	Distilled water	350	3.455	0.625	0.054	-	0.005	-
JLB1	Basalt	Distilled water	400	2.344	0.385	0.020	-	0.002	-
JLB1	Basalt	1 mol/L NaCl	200	30.517	764.660	12.202	4.472	0.042	0.676
JLB1	Basalt	1 mol/L NaCl	250	54.629	687.422	0.857	4.229	0.131	0.640
JLB1	Basalt	1 mol/L NaCl	300	40.015	459.802	0.319	2.509	0.152	-
JLB1	Basalt	1 mol/L NaCl	350	31.343	198.168	0.122	0.785	0.091	-
JLB1	Basalt	1 mol/L NaCl	400	24.114	156.936	0.050	0.042	0.035	-
THS-1	Granite	Distilled water	200	0.579	-	-	-	0.044	0.115
THS-1	Granite	Distilled water	250	1.572	0.047	-	-	0.087	0.142
THS-1	Granite	Distilled water	300	0.559	0.025	-	-	0.043	0.179
THS-1	Granite	Distilled water	350	0.656	-	-	-	0.055	-
THS-1	Granite	Distilled water	400	2.631	1.949	0.023	-	0.077	-
THS-1	Granite	1 mol/L NaCl	200	10.643	6.127	-	4.216	0.764	0.761
THS-1	Granite	1 mol/L NaCl	250	19.490	5.408	-	4.306	0.626	0.613
THS-1	Granite	1 mol/L NaCl	300	12.472	3.065	-	2.561	0.781	0.580
THS-1	Granite	1 mol/L NaCl	350	11.186	1.441	-	1.322	3.525	-
THS-1	Granite	1mol/L NaCl	400	8.705	0.723	0.151	0.361	3.373	-

Note: - means below the detection limit.

## 5. Discussion

### 5.1. Geochemical Characteristics

The total Na+K content, namely the Na<sub>2</sub>O+K<sub>2</sub>O content, is medium and high (7.52~9.08). In the SiO<sub>2</sub>–(Na<sub>2</sub>O+K<sub>2</sub>O) diagram (Figure 5A), granite samples are plotted in the granite field, indicating that the magma around the Jiangnan Basin has been differentiated to different degrees. In the SiO<sub>2</sub>–K<sub>2</sub>O diagram (Figure 5B), all the granite samples except the altered samples are plotted in the shoshonite series area, and all the other granite samples are plotted in the high-K calc-alkaline area. In A-CN-K compositional space, the aluminum saturation index ranges from 1.35 to 1.53, with an average of 1.45. All of the granites are strongly peraluminous. The AKI value of the over-alkaline index ranges from 0.70 to 0.83, with an average of 0.73, indicating that it is over-alkaline. According to previous studies, acidic and alkaline rocks are favorable for the accumulation of lithium [49]. Therefore, the granite on the periphery of the Jiangling Basin is favorable for the enrichment of lithium. Rb, Ba, and Zr are relatively enriched in the granites, showing the common characteristics of high-evolution granites in South China and indicating that the granites have undergone strong differentiation evolution.

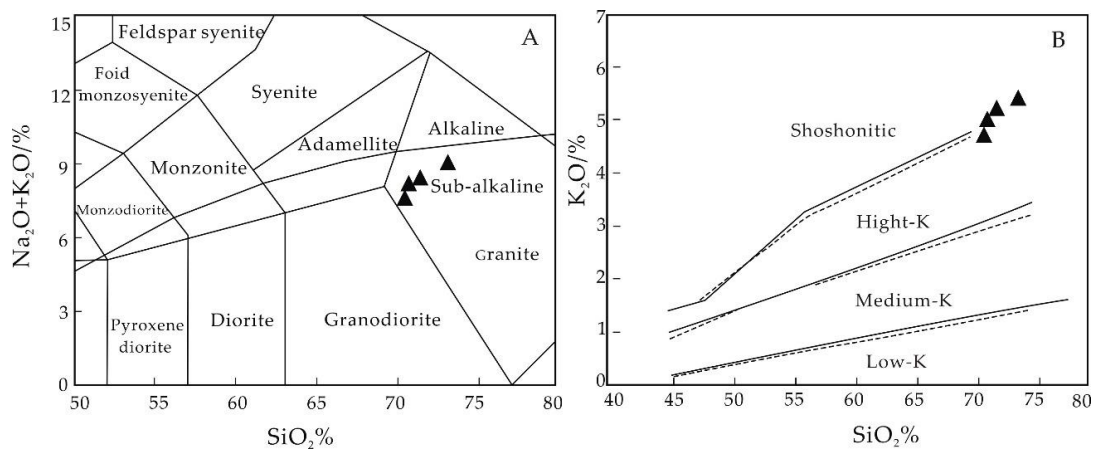


**Figure 5.** (A) SiO<sub>2</sub>–(Na<sub>2</sub>O+K<sub>2</sub>O) relation diagram in granite (modified from [50]); (B) SiO<sub>2</sub>–K<sub>2</sub>O relation diagram in granite (modified from [29]). The four triangles represent the Taohuashan granite samples.

According to the petrogeochemical characteristics of volcanic rocks, elemental analysis of basalt samples in the Jiangnan Basin (Table 2) and CIPW standard mineral calculations can be used to determine the specific types of basalt. As shown in Figure 6A, the samples are plotted in the basaltic andesite region of the sub-alkaline series. According to the calculation results of CIPW standard minerals by Yu et al. (1996) [51], the basalt can be further divided into three categories: quartz tholeiite, olivine tholeiite, and alkaline olivine basalt. They all belong to the sodic series and formed in a continental environment (Figure 6B–D). The basalts in the Jiangling depression are tholeiite- and potassium-rich basalts, which may provide abundant material sources for potassium-rich brine.

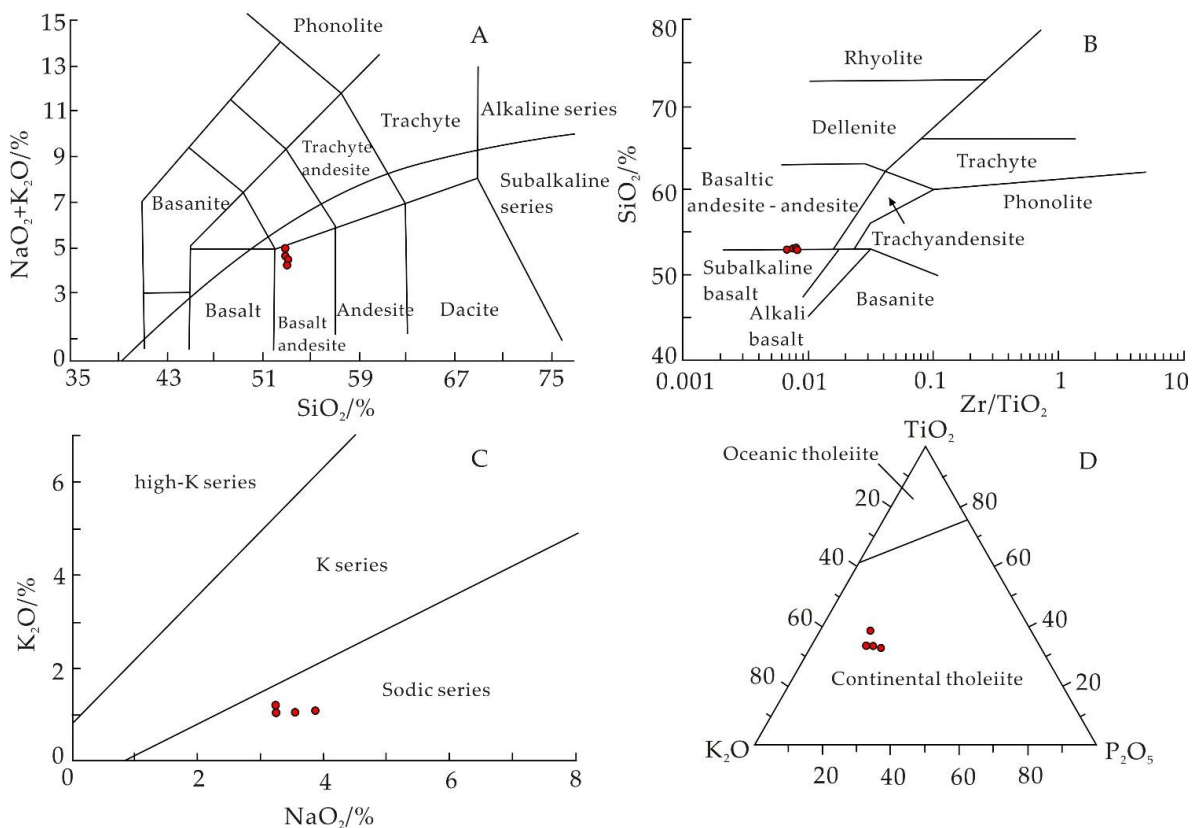


**Figure 6.** Classification diagram of volcanic rocks in Jiangling depression. (A) SiO<sub>2</sub>–(Na<sub>2</sub>O+K<sub>2</sub>O) relation diagram; (B) Zr/TiO<sub>2</sub>–SiO<sub>2</sub> relation diagram; (C) Na<sub>2</sub>O–K<sub>2</sub>O relation diagram; (D) TiO<sub>2</sub>–K<sub>2</sub>O–P<sub>2</sub>O<sub>5</sub> relation diagram. The four red dots represent basalt samples from Balingshan (after [52]).

### 5.2. Determination of the Starting and Stopping Temperatures of the Water–Rock Reaction

The homogenization temperature range of gas–liquid two-phase inclusions in granite varies greatly, with a concentration range of 170–230 °C and an average homogenization temperature of 210.1 °C, indicating that the fluid temperature of the water–rock reaction is high, and the lowest temperature of mineralization is 210.1 °C [53]. Therefore, the initial temperature of the water–rock reaction in igneous rock was set at 150–200 °C, and the experimental temperature range was set at 150–400 °C to explore the effect of the water–rock reaction on brine mineralization.

### 5.3. Discussion on the Genesis of Lithium–Potassium-Rich Brine

#### 5.3.1. Analysis of Static Immersion Experimental Results

The contents of K in the five fluids were different, but the trend was similar. Most of the K content in the solution was the highest after soaking for 55 h after the seventh sampling. Moreover, weakly alkaline (pH = 8) solutions and 1 mol/L and 2 mol/L NaCl solutions were more conducive to K leaching (Figure 7). At room temperature, the content of K in the 2 mol/L NaCl was higher than that in the 1 mol/L NaCl solution, and the dissolution amount of K in the 1 mol/L of NaCl solution was 10.90 mg/L. However, its concentration increased with increasing salinity and soaking time. In the 2 mol/L NaCl solution, the maximum value was 14.86 mg/L. Basalt immersion was more conducive to potassium dissolution than granite, and the dissolution amount was one order of magnitude higher (Table 4).

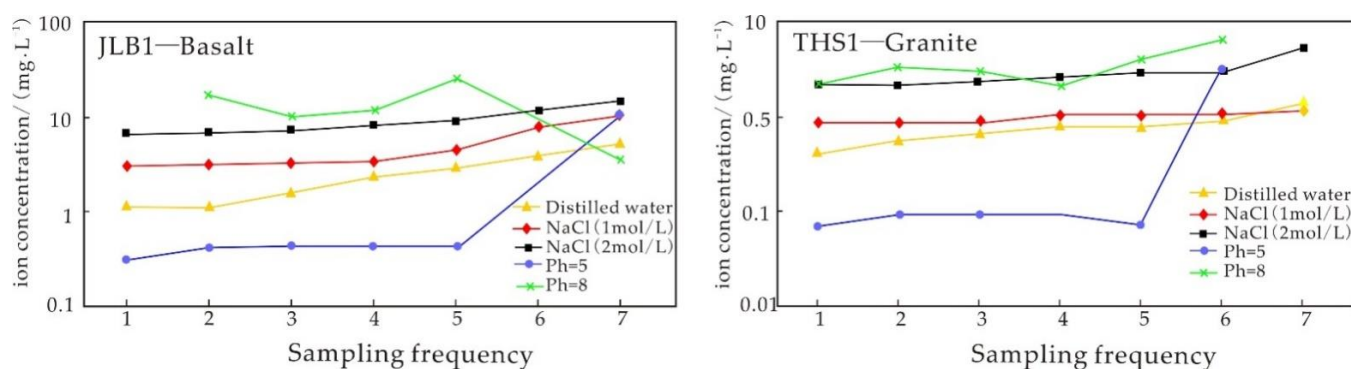


Figure 7. Variation diagram of K ion concentration in igneous rock static immersion experiment.

Ca, Mg, and Sr showed a consistent trend, with the highest element content in the 1 mol/L and 2 mol/L NaCl solutions, followed by the solution with pH = 5; the lowest element content was in the distilled water and the solution with pH = 8 (Figures 8–10), in which the content of Ca was the highest, followed by Mg, and the lowest was Sr. With increasing soaking time, the dissolution amount of the three kinds of ions increased slowly. At room temperature, the Ca, Mg, and Sr contents in 2 mol/L NaCl were generally higher than those in 1 mol/L NaCl solution. In the 1 mol/L NaCl solution, the maximum Ca dissolution amount was 290.40 mg/L, and the concentration of Ca increased with increasing salinity and immersion time. The maximum value of Ca in the 2 mol/L NaCl solution was 343.45 mg/L. In the 1 mol/L NaCl solution, the maximum Mg dissolution was 18.97 mg/L, while in the 2 mol/L NaCl solution, the maximum Mg dissolution was 22.79 Mg/L. In 1 mol/L NaCl solution, the maximum Sr release was 1.59 mg/L, while in the 2 mol/L NaCl solution, the maximum Sr release was 1.90 mg/L (Table 4).

No concentration of lithium was detected in the five fluids.

Br, I, and B were not detected in distilled water, pH = 5, and pH = 8 solutions but were detected in the 1 mol/L and 2 mol/L NaCl solutions. The changes in Br, I, and B in 1 mol/L and 2 mol/L NaCl solutions are discussed as follows:

The Br content fluctuated within a certain range with little change (Figure 11). In addition, the Br content in the 2 mol/L NaCl solution was 1–2 times higher than that in the 1 mol/L NaCl solution (Table 4).

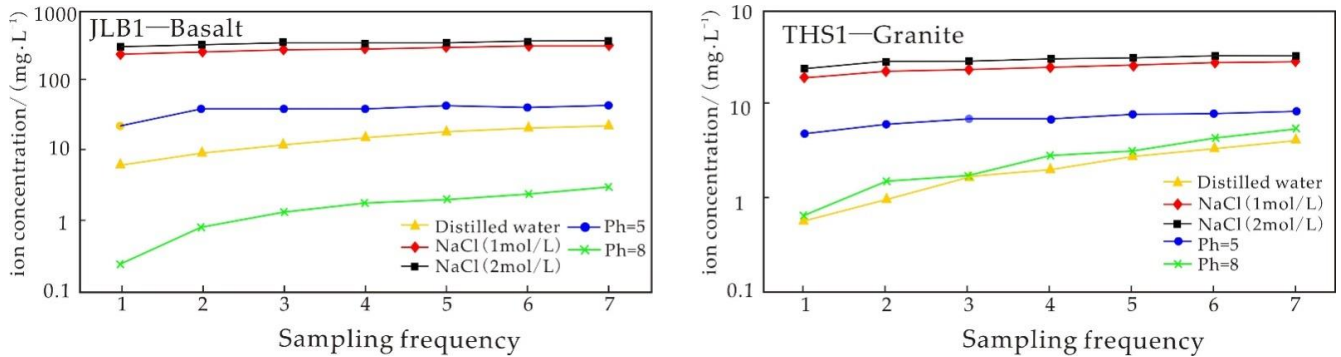


Figure 8. Variation diagram of Ca ion concentration in igneous rock static immersion experiment.

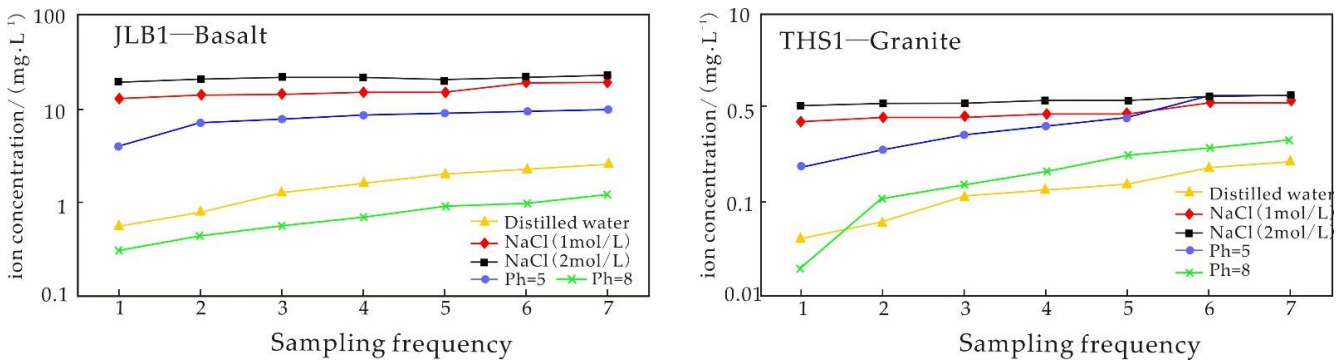


Figure 9. Variation diagram of Mg ion concentration in igneous rock static immersion experiment.

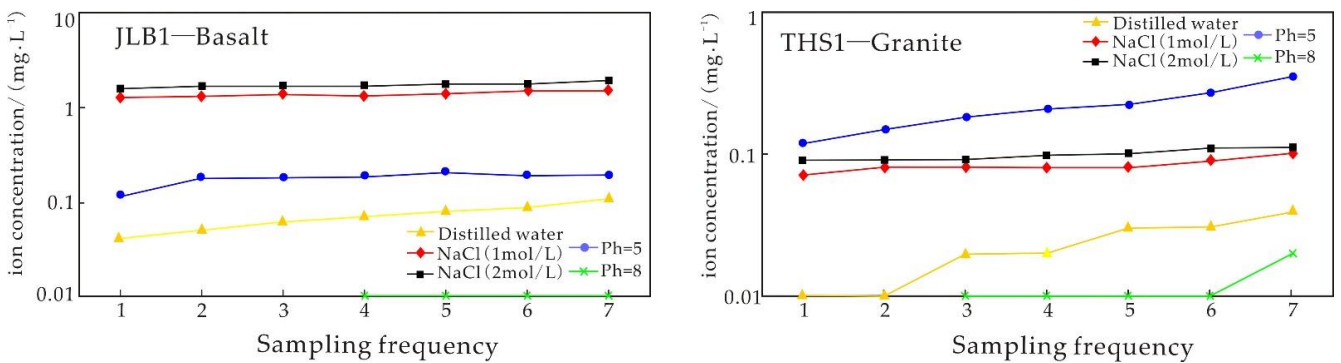


Figure 10. Variation diagram of Sr ion concentration in igneous rock static immersion experiment.

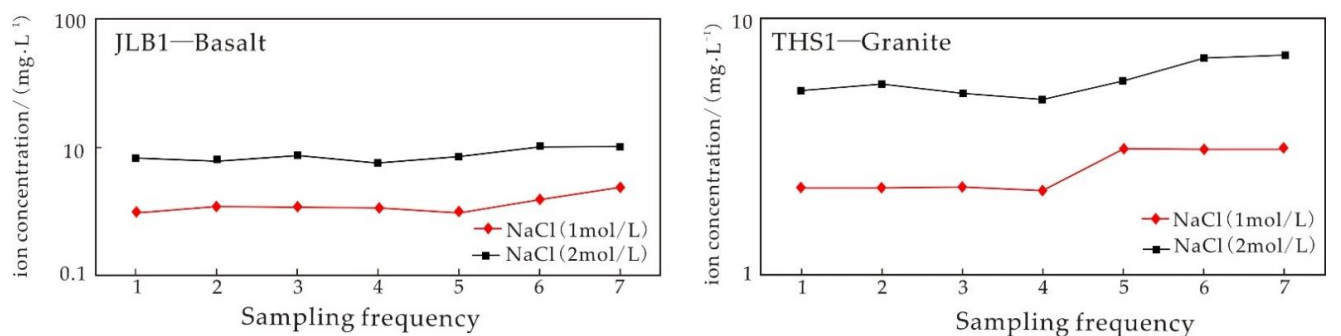


Figure 11. Variation diagram of Br ion concentration in igneous rock static immersion experiment.

The I and B contents in the solution were low with little fluctuation, but the saline fluid more easily activated the ions (Figures 12 and 13). Moreover, the activation effect of the 2 mol/L NaCl solution was better than that of the 1 mol/L NaCl solution; it was generally 1~2 times higher (Table 4).

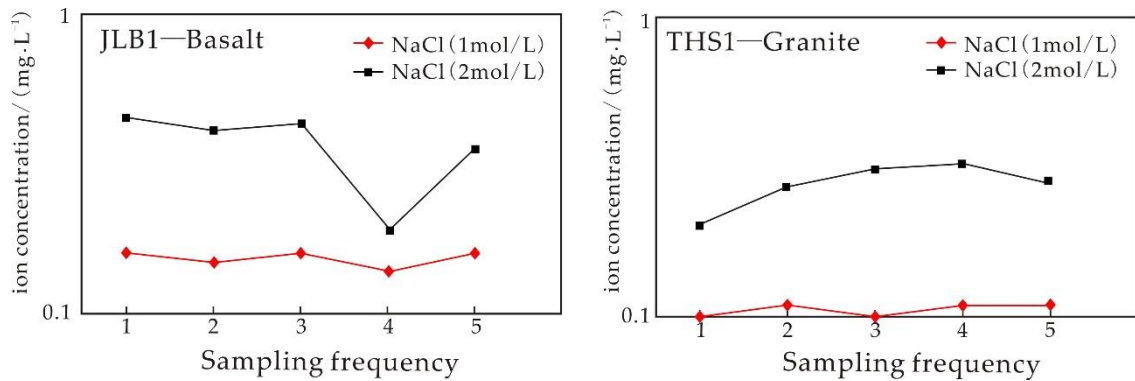


Figure 12. Variation diagram of I ion concentration in igneous rock static immersion experiment.

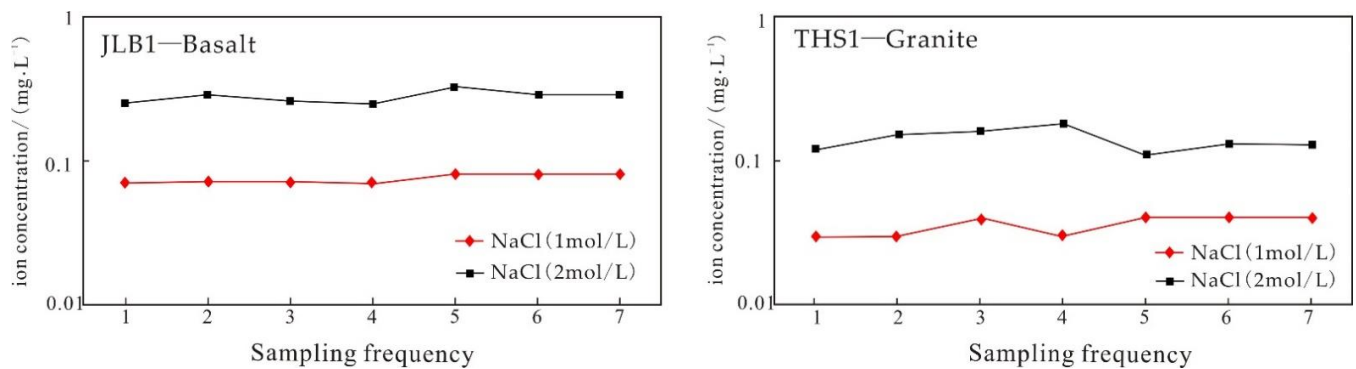


Figure 13. Variation diagram of B ion concentration in igneous rock static immersion experiment.

The above analysis shows that saline fluid was more conducive to the activation of various ions, especially in the 2 mol/L NaCl solution, while the solution with weak acid was conducive to the dissolution of K. Li was not dissolved in the whole experiment, indicating that the solution concentration was not the factor affecting the dissolution of lithium, and the main controlling factor was temperature. Under the same conditions, the solubility of K in the NaCl solution was approximately 1~2 orders of magnitude higher than that in the distilled water. Potassium in basalt is more easily dissolved than that in granite, which further reveals that the water–rock reaction between basalt and basin brine with weak alkalinity can provide the source of ore-forming materials for potassium-rich brines.

### 5.3.2. Influence of Time on the Igneous Rock Water–Rock Reaction

The trends of dissolution of Ca, K, Sr, and Li elements in basalt and granite are the same, with a small fluctuation and obvious positive correlation (Figure 14). Under certain conditions, Mg in granite is correlated with S, while Mg in basalt is negatively correlated with Ca, K, Sr, and Li. The maximum dissolution amounts of K, Li, Mg, Ca, and S are reached after 3 h of reaction, and the maximum dissolution amount of K, Mg, S, and Br in granite is reached after 5 h of reaction (Figure 14). The result of this reaction is quite different from that of the brine samples in the Jiangling Basin, which indicates that the formation of brine ore takes a long time.

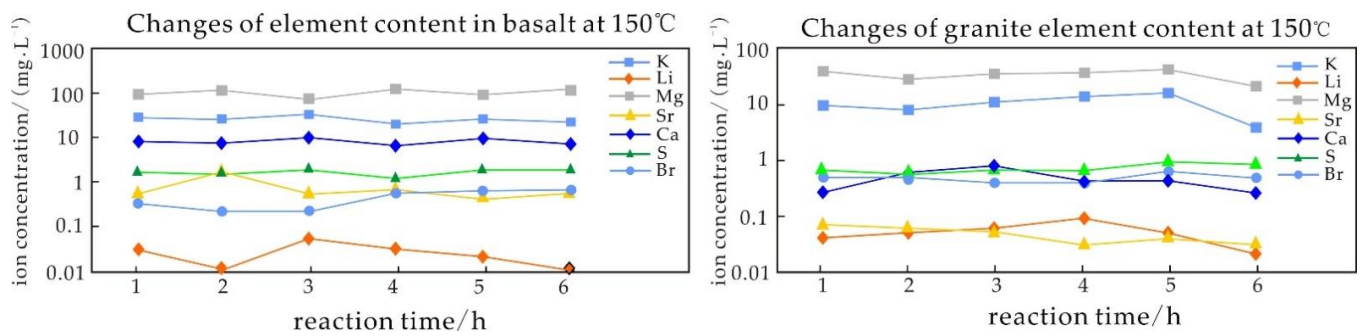


Figure 14. Diagram of element content over time in igneous rock water–rock reaction.

### 5.3.3. Influence of Temperature on the Igneous Rock Water–Rock Reaction

Considering the elemental composition of the original rock, whether the reaction fluid medium was distilled water or 1 mol/L NaCl solution, K dissolution in basalt reached a relatively high value at 250 °C, and the dissolution decreased with increasing temperature. At 400 °C, the dissolution reached the lowest maximum value, 54.629 mg/L (Figure 15). The amount of K in the same fluid was different at different temperatures. At the same temperature, the K dissolution amount in 1 mol/L NaCl solution was higher than that in distilled water. The dissolution amount of Li in basalt was very low, whether the reaction fluid medium was distilled water or 1 mol/L NaCl solution; it reached a maximum value of 0.152 mg/L at 250–300 °C, with a small fluctuation, and then it decreased gradually with increasing temperature (Figure 16).

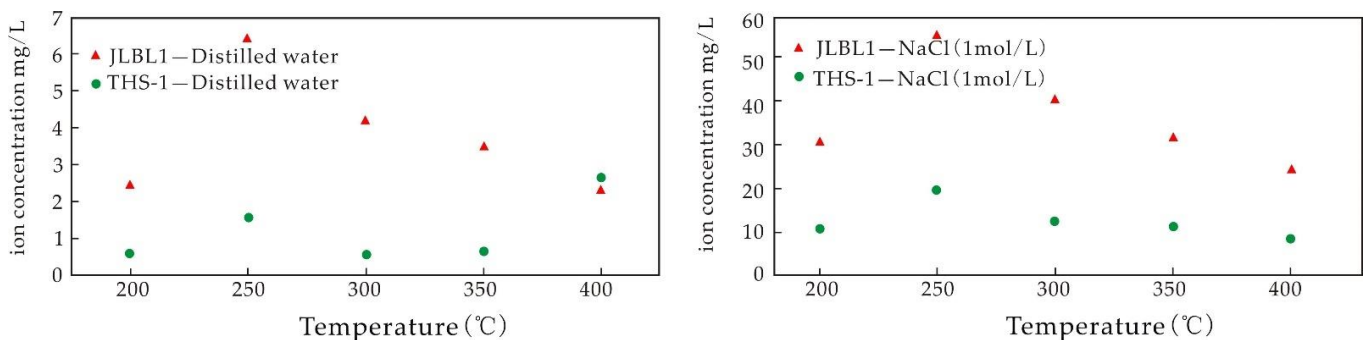


Figure 15. Diagram of K ion content over temperature in water–rock reaction.

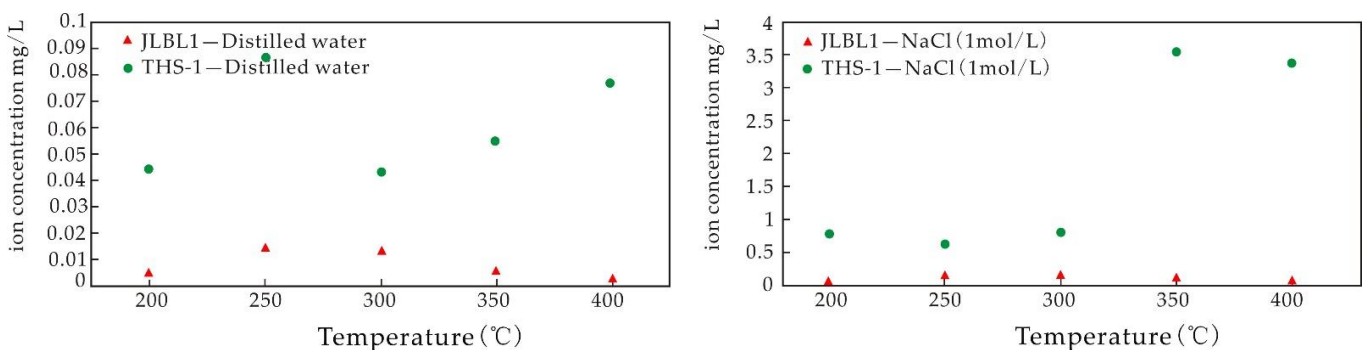


Figure 16. Diagram of Li ion content over temperature in water–rock reaction.

Considering the elemental composition of the original rock, whether the reaction fluid medium was distilled water or 1 mol/L NaCl solution, Li dissolution in basalt and granite reached a relatively high value at 250 °C, and the dissolution decreased with increasing temperature. At 400 °C, the dissolution reached the lowest maximum value, 19.490 mg/L (Figure 16). The amount of Li in the same fluid was different at different temperatures. At

the same temperature, the Li dissolution amount in the 1 mol/L NaCl solution was higher than that in distilled water. The dissolved Li from granite was an order of magnitude higher than that from basalt, whether the reaction fluid medium was distilled water or 1 mol/L NaCl solution; it reached the maximum value of 3.525 mg/L at 250–350 °C, with a large fluctuation, and then it decreased gradually with increasing temperature (Figure 16).

The contents of Ca, Mg, and Sr in the 1 mol/L NaCl solution and distilled water decreased with increasing temperature, and the decreasing rate of Mg was higher than that of Ca and Sr (Figure 17). However, the content of various ions in 1 mol/L NaCl solution was higher than that in distilled water. The content of Br in the fluid was different at different temperatures. At the same temperature, the content of Br ions in 1 mol/L NaCl solution was higher than that in distilled water (Figure 17).

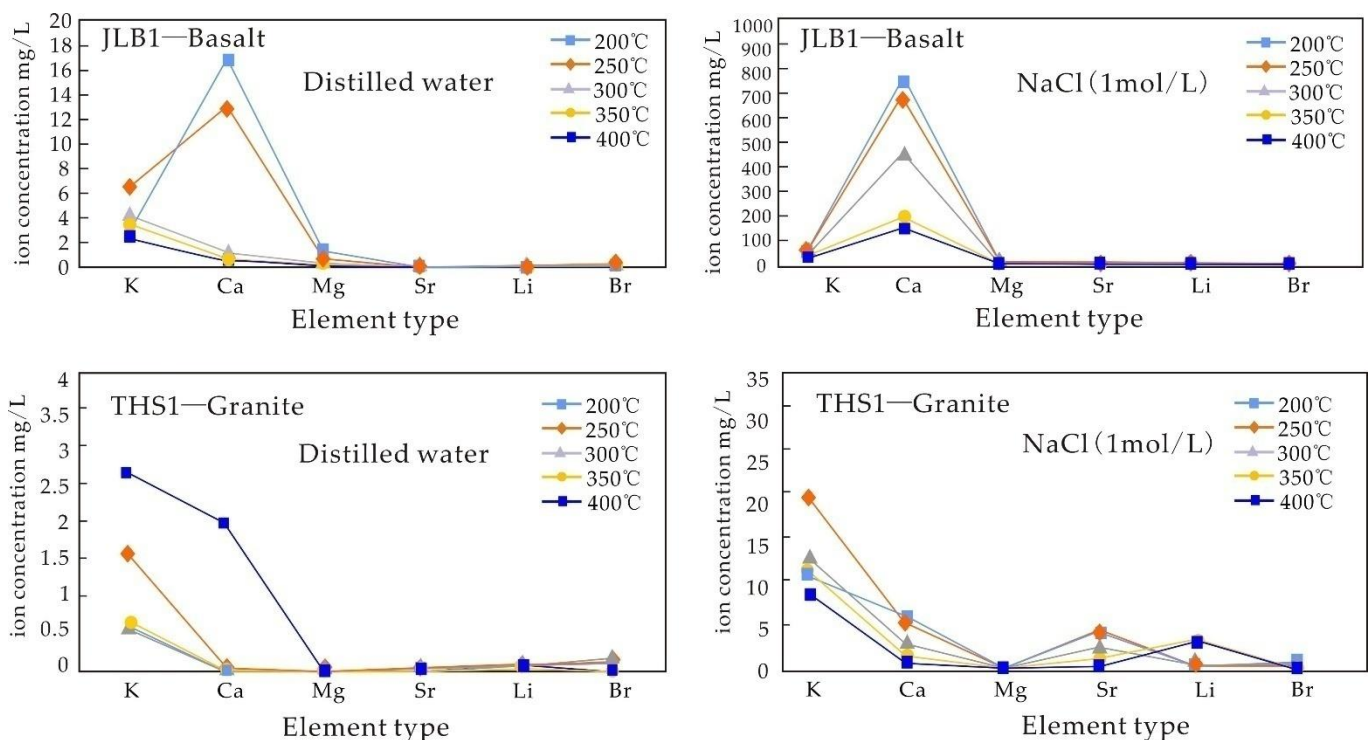


Figure 17. Diagram of ionic concentration over temperature in water–rock reaction.

The above analysis shows that the rates of water–rock reactions are different at different temperatures for the same fluid. The dissolution rates of Ca, Mg, and Sr decrease with increasing temperature, while the dissolution rates of K and Li first increase and then decrease with the increase in temperature. The change of Br is not obvious (Figure 17). However, the content of each element in the saline fluid is much higher than that in the distilled water, indicating that the saline fluid more easily activates ions. Basalt is favorable for the dissolution of potassium, and granite is favorable for the dissolution of lithium.

#### 5.3.4. Influence of Fluid Composition on the Igneous Rock Water–Rock Reaction

The dissolution of K in both basalt and granite is approximately 10 times higher in distilled water than in NaCl solution, and it is positively correlated with concentration (Figure 18). The dissolution amount of Ca increases with increasing salinity (Figure 18). The dissolution amount of Mg in granite is small. The dissolution amount of Sr increases with increasing concentration. The dissolution amount of Li is low in basalt and approximately one order of magnitude smaller than that in granite. Basalt is not the main source of lithium in brine. Under the same conditions, the leaching capacity of NaCl solution for various elements in rock is approximately 1–2 orders of magnitude higher than that of

deionized water (Figure 18), indicating that high-salinity fluid is the main migration carrier of ore-forming elements.

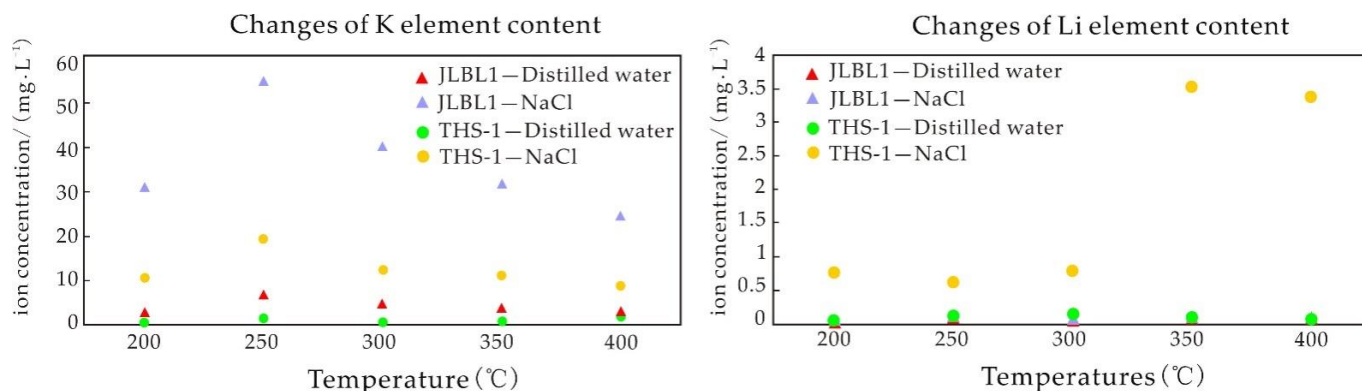


**Figure 18.** Diagram of K and Li element content in distilled water and NaCl solution over temperature in water–rock reaction.

Compared with leaching results under normal temperatures and the chemical analysis results of Jiangnan basin brine (Table 4), the dissolution of Li, K, Sr, Mg, and other elements in autoclave water–rock reactions is significantly higher than the normal temperature immersion results, but still two orders of magnitude lower than the element content in the basin brine, indicating that high temperatures are more favorable for K, Li, Na, and Sr enrichment. The process with higher-than-normal temperatures has a significant impact on the composition of fluid, which is favorable for igneous rocks to react and provide material source for brine. Water–rock reaction of igneous rock is one of the important processes for the mineralization of lithium–potassium-rich brine, and surface evaporation and concentration are the main mechanisms for the mineralization of brine.

### 5.3.5. Geotectonics

According to Guan [51], Mesozoic volcanic rocks in eastern China are divided into four rock belts extending to the NNE. According to the research results of Xu et al. (2015) [54], volcanic activity in the Paleogene was mainly distributed in the NE-trending Songliao Plain, North China Plain, and Jiangnan Plain. The thickest basalt was more than 1000 m thick, and the magma was mainly tholeiitic basaltic magma, which was only sporadically exposed on the surface. From the Cretaceous to the Paleocene, a large-scale lithospheric extension characterized by volcanic activity, rift basin formation, and large-scale mineralization occurred in North China [32,55,56]. At the same time, due to the extension of the lithosphere, there were also large-scale faulted basins, volcanic eruptions, and metallogenic accumulations in Central China and South China [57].

Volcanic rocks are widely distributed in the Jiangnan Basin, with a total area of 5049 km<sup>2</sup>, accounting for 18% of the basin area. Volcanic rocks are well developed in the Jiangling depression, with a distribution area of 3527 km<sup>2</sup> (Figure 4), accounting for nearly half of the whole depression, and an average thickness of more than 200 m from the Shashi Formation to Qianjiang Formation [35,58]. Some basalt samples collected in the Balingshan area are typical tholeiites of continental rift type, which are rich in K, Li, Rb, Sr, Zn, Cu, and other elements [59].

Most scholars believe that the composition of magma is mainly controlled by the composition of the source region, and asthenosphere–lithosphere interactions lead to the heterogeneity in the source region. Tholeiitic basalts are the result of a relatively high degree of melting at the shallow part of the lithospheric mantle or asthenospheric mantle [60,61]. Intracontinental tholeiitic basalts generally have high boron contents, ranging from  $0.48 \times 10^{-6}$  to  $17.8 \times 10^{-6}$  [62]. As a soluble element, boron can be released in large quantities into surface hot springs, concentrated brines, and meteoric water. Along with the large-scale volcanic eruption in the Paleocene in the Jiangling depression, a large

number of boron-containing minerals carried by magma and post-stage hydrothermal fluids could have provided a large number of ore-forming materials for brine deposits in the Jiangling depression.

### 5.3.6. Paleocene Paleoclimate and Paleo-Lake Composition

The sedimentary environment of Paleocene salt-bearing strata in the Jiangling depression was dominated by a warm and dry environment, which alternated frequently with a humid environment. Under the paleogeomorphic background of “high mountain and deep basins”, the brine in the lake basin reached sodium chloride saturation through strong evaporation (extremely dry and hot climate events), and halite precipitated. The brines continued to be evaporated to form boron-rich brines, and with the length of salt-forming time, halite layers with different thicknesses formed. The Paleocene–Eocene salt-bearing strata in the Jiangling depression are characterized by mineral deposits such as mudstone, silt or fine sandstone, marl, halite, anhydrous mirabilite, calcium mirabilite, anhydrite, potassic gypsum, potassic salt, and carnallite [3,6], which are mineralogical markers of a hot and dry climate.

The long-term subsidence of the Jiangling depression leads to good basin sealing. During the Paleocene, the Jiangling depression was volcanically active, which brought abundant ore-forming materials for brine mineralization into the depression. However, the contents of lithium and potassium in the brine in the Jiangling depression are abnormally high and reach the industrial grade. Water–rock reactions alone could not have made the concentration of ore-forming fluid reach such a high level, which is inseparable from the continuous enrichment of minerals caused by evaporation and concentration in late ancient lakes under extremely dry and hot climate conditions. The formation of boron-rich brines in the Jiangling depression is the coupled result of structural conditions, material conditions, and an arid climate.

## 6. Conclusions

- (1) The field evidence shows that Mesozoic and Cenozoic igneous rocks in the Jiangling depression are mainly basalt and granite, and their distribution area is more than half of the basin area. The magma is differentiated to different degrees, which could have provided lithium and potassium for the brine.
- (2) The static immersion experiment at room temperature shows that saline fluid is more likely to activate K ions in basalt. The weak alkaline solution more easily dissolves K. During the whole experiment, Li was not dissolved, indicating that the concentration of the solution was not the factor affecting the dissolution of lithium, and the main controlling factor was temperature.
- (3) The experiments of water–rock reaction with high temperature show that the dissolution rates of Ca, Mg, and Sr decrease with the increase in temperature, while the dissolution rates of K and Li first increase and then decrease with the increase in temperature. The dissolution of K and Li is easier when saline fluid reacts with volcanic rock. The dissolution rate of K in basalt is higher than that of Li, and that of Li in granite is higher than that of K. Compared with the results at normal temperatures, the ability of the fluid to leach elements is significantly enhanced at higher temperatures, the temperature is the main factor controlling the ability to leach elements, and the high-salinity fluid is the main migration carrier of ore-forming elements.
- (4) According to the experiments of water–rock reaction, the mineral composition of the ancient brine in the Jiangling depression during the Paleogene is consistent with that of the brine found today, indicating that the Jiangling depression in the Paleogene was influenced by hot and dry climate. However, these two compositions are different by a few orders of magnitude, indicating that the formation of lithium–potassium-rich brines requires a long period of time. The water–rock reaction is one of the important processes for brine formation, and surface evaporation and concentration are the main mechanisms for brine mineralization.

**Author Contributions:** C.W. and X.Y. designed the research and prepared the original manuscript. R.L. and L.L. revised the manuscript. K.Y. and C.Y. participated in sample collection and processing. All authors have read and agreed to the published version of the manuscript.

**Funding:** The work was supported by the Central Public Welfare Scientific Research Basic Scientific Research Business Expenses (Nos. KK2005 and KY1603), the National Natural Science Foundation of China (Nos. U20A2092, 42002106, 41907262, and 41502089), the National Basic Research Program of China (973 program) (No. 2011CB403007), and the China Geological Survey (No. DD20190606).

**Institutional Review Board Statement:** Not applicable.

**Informed Consent Statement:** Not applicable.

**Data Availability Statement:** Data are available based on request.

**Acknowledgments:** We would like to thank Kuan Zhang and Cheng Chen from Jinhui (Jing Zhou) Fine Chemical Co., Ltd. for their help during the field sampling. We are grateful to reviewers for their critical and constructive review.

**Conflicts of Interest:** The authors declare that they have no conflict of interest.

## Abbreviations

Pl Plagioclase  
Px Pyroxene

## References

1. Kesler, S.E.; Gruber, P.W.; Medina, P.A.; Keoleian, G.A.; Wallington, T.J. Global lithium resources: Relative importance of pegmatite, brine and other deposits. *Ore Geol. Rev.* **2012**, *48*, 55–69. [[CrossRef](#)]
2. Godfrey, L.V.; Chan, L.H.; Alonso, R.N.; Lowenstein, T.K.; McDonough, W.F.; Houston, J.; Li, J.; Bobst, A.; Jordan, T.E. The role of climate in the accumulation of lithium-rich brine in the central Andes. *Appl. Geochem.* **2013**, *38*, 92–102. [[CrossRef](#)]
3. Wang, C.L.; Liu, C.L.; Liu, B.K.; Shen, L.J.; Cai, X.L.; Yu, X.C.; Xie, T.X.; Wang, L.C.; Zhao, Y.J.; Xuan, Z.Q. The discovery of carnallite in Paleocene Jiangling Depression and its potash searching significance. *Acta Geol. Sin.* **2015**, *89*, 129–136.
4. Yu, X.C.; Wang, C.L.; Liu, C.L.; Zhang, Z.C.; Xu, H.M.; Huang, H.; Xie, T.X.; Li, H.N.; Liu, J.L. Sedimentary characteristics and depositional model of a Paleocene-Eocene salt lake in the Jiangling Depression, China. *Chin. J. Oceanol. Limn.* **2015**, *33*, 1426–1435. [[CrossRef](#)]
5. Liu, C.L.; Yu, X.C.; Zhao, Y.J.; Wang, J.Y.; Wang, L.C.; Xu, H.M.; Li, J.; Wang, C.L. Tentative discussion on regional metallogenetic background and mineralization mechanism of subterranean brines rich in potassium and lithium in South China Block. *Miner. Depos.* **2016**, *35*, 1119–1143.
6. Wang, C.L.; Liu, C.L.; Yu, X.C.; Li, H.N.; Liu, J.L. The extremely hot and dry climatic events and potash enrichment in salt lakes. *Acta Geol. Sin.-Engl.* **2016**, *90*, 769–770.
7. Zeng, F.M.; Xiang, S.Y. Geochronology and Mineral Composition of the Pleistocene Sediments in Xitaijin air Salt Lake Region, Qaidam Basin: Preliminary Results. *J. Earth Sci.* **2017**, *8*, 622–627. [[CrossRef](#)]
8. Wang, D.H.; Liu, L.J.; Dai, H.Z.; Liu, S.B.; Hou, J.L.; Wu, X.S. Discussion on particularity and prospecting direction of large and super-large spodumene deposits. *Earth Sci.* **2017**, *42*, 2243–2257.
9. Shen, C.B.; Mei, L.F.; Min, K.; Jonckheere, R.; Ratschbacher, L.; Yang, Z.; Peng, L.; Liu, Z. Multi-chronometric dating of the Huarong granitoids from the middle Yangtze Craton: Implications for the tectonic evolution of eastern China. *J. Asian Earth Sci.* **2012**, *52*, 73–87. [[CrossRef](#)]
10. Li, R.Q.; Liu, C.L.; Jiao, P.C.; Wang, J.Y. The tempo-special characteristics and forming mechanism of Lithium-rich brines in China. *China Geol.* **2018**, *1*, 72–83. [[CrossRef](#)]
11. Munk, L.A.; Boutt, D.F.; Hyneck, S.; Moran, B. Hydrogeochemical fluxes and processes contributing to the formation of lithium-enriched brines in a hyper-arid continental basin. *Chem. Geol.* **2018**, *493*, 37–57. [[CrossRef](#)]
12. Li, R.Q.; Liu, C.L.; Xu, H.M.; Jiao, P.C.; Hu, Y.F.; Li, F.; Sun, X.H. Genesis of glauberite sedimentation in Lop Nur Salt Lake—Constraints from thermo dynamics imulation of the shallow ground water in the Tarim River Basin, China. *Chem. Geol.* **2020**, *537*, 119461. [[CrossRef](#)]
13. Rosenthal, E.; Möller, P.; Buch-Leviatan, O.; Politi, M. The Hydrogeochemical Stratigraphy of Brines and Its Implications on Water Management in the Central Jordan-Dead Sea Rift Valley, Israel. *Geofluids* **2020**, *17*, 9812597.
14. Godfrey, L.V.; Álvarez-Amado, F. Volcanic and Saline Lithium Inputs to the Salar de Atacama. *Minerals* **2000**, *10*, 201. [[CrossRef](#)]
15. Wang, C.L.; Liu, L.H.; Li, Q.; Meng, L.Y.; Liu, C.L.; Zhang, Y.Y.; Wang, J.Y.; Yu, X.C.; Yan, K. Petrogeochemical characteristics and genetic analysis of the source area of briny lithium-potassium ore in Jitai Basin of Jiangxi province. *Acta Petrol. Mineral.* **2020**, *39*, 65–84.

16. Liu, C.L.; Wang, M.L.; Jiao, P.C.; Chen, Y.Z. The exploration experiences of pot ash deposits in the world and probing of countermeasures of China's future pot ash-deposits investigation. *Geol. Chem. Miner.* **2006**, *28*, 1–8.
17. Munk, L.A.; Hynek, S.A.; Bradley, D.C.; Boutt, D.; Labay, K.; Jochens, H. Lithium Brines: A Global Perspective. *Rev. Econ. Geol.* **2016**, *18*, 339–365.
18. Lowenstein, T.K.; Spencer, R.J.; Zhang, P.X. Origin of Ancient Potash Evaporites: Clues from the Modern Nonmarine Qaidam Basin of Western China. *Science* **1989**, *245*, 1090–1092. [[CrossRef](#)]
19. Holmearda, J.G.; Hutchinsan, R.W. Potash-bearing evaporates in the Danakil area, Ethiopia. *Econ. Geol.* **1968**, *63*, 129–132.
20. Arod, A. Mineral spring and saline lake of the western rift Valley, Uganda. *Geochim. Cosmochim. Acta* **1969**, *10*, 1152–1162. [[CrossRef](#)]
21. Yu, X.C.; Liu, C.L.; Wang, C.L.; Zhao, J.X.; Wang, J.Y. Origin of geothermal waters from the Upper Cretaceous to Lower Eocene strata of the Jiangling Basin, SouthChina: Constraints by multi-isotopic tracers and water-rock interactions. *Appl. Geochem.* **2020**, *124*, 104810. [[CrossRef](#)]
22. Munk, L.; Chamberlain, C.P. Lithium Brine Resources: A Predictive Exploration Model, U.S. Geological Survey, Mineral Resources External Research Program-Final Technical Report: G10AP00056.2011. Available online: <http://minerals.usgs.gov/mrerp/reports/Munk-G10AP00056> (accessed on 8 November 2021).
23. Hofstra, A.H.; Todorov, T.I.; Mercer, C.N.; Adams, D.T.; Marsh, E.E. Silicate melt inclusion evidence for extreme pre-eruptive enrichment and post-eruptive depletion of lithium in silicic volcanic rocks of the western United States: Implications for the origin of lithium-rich brines. *Econ. Geol.* **2013**, *108*, 1691–1701. [[CrossRef](#)]
24. Von Strandmann, P.A.P.; Frings, P.J.; Murphy, M.J. Lithium isotope behavior during weathering in the Ganges Alluvial Plain. *Geochim. Cosmochim. Acta* **2017**, *198*, 17–31. [[CrossRef](#)]
25. Price, J.G.; Lechler, P.J.; Lear, M.B.; Giles, T.F. Possible Volcanic Source of Lithium in Brines in Clayton Valley, Nevada. *Geology and Ore Deposits 2000: The Great Basin and Beyond Proceedings: Geological Society of Nevada Symposium Proceedings: Nevada, USA, 2000*. pp. 241–248. Available online: <https://www.gsnv.org/shop/geology-and-ore-deposits-2000-the-great-basin-and-beyond-symposium-proceedings/> (accessed on 23 November 2021).
26. Araoka, D.; Kawahata, H.; Takagi, T.; Watanabe, Y.; Nishimura, K.; Nishio, Y. Lithium and strontium isotopic systematics in playas in Nevada, USA: Constraints on the origin of lithium. *Miner. Depos.* **2013**, *49*, 371–379. [[CrossRef](#)]
27. Li, R.Q.; Liu, C.L.; Chen, X.; Chen, Y.Z.; Wang, C.L. Salting law by cooling deep potassium-bearing brine in Jiangling depression. *J. Salt Lake Res.* **2013**, *21*, 1–6.
28. Li, R.Q.; Chen, X.; Liu, C.L.; Ma, L.C. Study on loss mechanism of rubidium during potassium crySTALLIZATION from potassium-rich brine of Jiangling sunken area. *Inorg. Chem. Ind.* **2014**, *46*, 18–20, 26.
29. Peccerillo, R.; Taylor, S.R. Geochemistry of Eocene calc-alkaline volcanic rocks from the Kastamonu area, Northern Turkey. *Contrib. Mineral. Petr.* **1976**, *58*, 63–81. [[CrossRef](#)]
30. Risacher, F.; Alonso, H.; Salazar, C. The origin of brines and salts in Chilean salars: A hydrochemical review. *Earth-Sci. Rev.* **2003**, *63*, 249–293. [[CrossRef](#)]
31. Zhou, X.; Jiang, C.L.; Han, J.J.; Tang, L.W.; Cao, Q.; Li, T. Some problems related to the evaluation of subsurface brine resources in deep-seated aquifers in sedimentary basins. *Acta Geol. Sin.* **2013**, *34*, 610–616.
32. Gilder, S.A.; Keller, G.R.; Luo, M.; Goodell, P.C. Timing and spatial distribution of rifting in China. *Tectonophysics* **1991**, *197*, 225–243. [[CrossRef](#)]
33. Yu, X.Q.; Shu, L.S.; Deng, P.; Wang, B.; Zu, F.P. The sedimentary features of the Jurassic-Tertiary terrestrial strata in southeast China. *J. Stratigr.* **2003**, *27*, 224–263.
34. Zhang, Y.Q.; Zhao, Y.; Dong, S.W.; Yang, N. Tectonic evolution stages of the Early Cretaceous rift basins in Eastern China and adjacent areas and their geodynamic background. *Front. Earth Sci.-Front.* **2004**, *11*, 123–133.
35. Xu, L.X.; Yan, C.D.; Yu, H.L.; Wang, B.Q.; Yu, F.Q.; Wang, D.F. Chronology of Paleogene volcanic rocks in Jiangnan Basin. *Oil Gas Geol.* **1995**, *16*, 132–137.
36. Schellart, W.P.; Lister, G.S. The role of the East Asian active margin in widespread extensional and strike-slip deformation in East Asia. *J. Geol. Soc. Lond.* **2005**, *162*, 959–972. [[CrossRef](#)]
37. Zhu, R.X.; Xu, Y.G.; Zhu, G.; Zhang, H.F.; Zheng, T.Y. Destruction of the North China Craton. *Sci. China (Ser. D)* **2012**, *55*, 1565–1587. [[CrossRef](#)]
38. Liu, S.F.; Steel, R.; Zhang, G.W. Mesozoic sedimentary basin development and tectonic implication, northern Yangtze Block, eastern China: Record of continent–continent collision. *J. Asian Earth Sci.* **2005**, *25*, 9–27. [[CrossRef](#)]
39. Shen, C.B.; Donelick, R.A.; O'Sullivan, P.B.; Jonckheere, R.; Yang, Z.; She, Z.B.; Miu, X.L.; Ge, X. Provenance and hinterland exhumation from LA-ICP-MS zircon U–Pb and fission-track double dating of Cretaceous sediments in the Jiangnan Basin, Yangtze block, central China. *Sediment. Geol.* **2012**, *281*, 194–207. [[CrossRef](#)]
40. Teng, X.H.; Fang, X.M.; Kaufman, A.J.; Liu, C.L.; Wang, J.Y.; Zan, J.B.; Yang, Y.B.; Wang, C.L.; Xu, H.M.; Schulte, R.F.; et al. Sedimentological and mineralogical records from drill core SKD1 in the Jiangnan Basin, Central China, and their implications for late Cretaceous–early Eocene climate change. *J. Asian Earth Sci.* **2019**, *182*, 103936. [[CrossRef](#)]
41. Wang, C.L.; Meng, L.Y.; Liu, C.L.; Yu, X.C.; Yan, K.; Liu, S.H.; You, C.; Li, K.K.; Teng, X.H. Study on the genesis of Paleocene underground brine-boron deposit in Jiangling Depression. *Acta Petrol. Mineral.* **2021**, *40*, 1–13.

42. Wang, B.J.; Lin, C.S.; Chen, Y.; Lu, M.G.; Liu, J.Y. Episodic tectonic movement and evolutionary character in Jiangnan basin. *Oil Geophys. Prospect.* **2006**, *41*, 226–230.
43. Wang, C.L.; Liu, C.L.; Wang, J.Y.; Yu, X.C.; Yan, K. Palynology and stratigraphy of the thick evaporate-bearing Shashi Formation in Jiangling Depression, Jiangnan Basin of South China, and its paleoclimate change. *China Geol.* **2020**, *2*, 283–291.
44. Shen, C.B.; Mei, L.F.; Peng, L.; Chen, Y.Z.; Yang, Z.; Hong, G.F. LA-ICPMS U–Pb zircon age constraints on the provenance of Cretaceous sediments in the Yichang area of the Jiangnan Basin, central China. *Cretac. Res.* **2012**, *34*, 172–183. [[CrossRef](#)]
45. Liu, J.H.; Zhang, P.Z.; Lease, R.O.; Zheng, D.; Wan, J.; Wang, W.; Zhang, H. Eocene onset and late Miocene acceleration of Cenozoic intracontinental extension in the North Qinling range–Weihe graben: Insights from apatite fission track thermochronology. *Tectonophysics* **2013**, *584*, 281–296. [[CrossRef](#)]
46. Xu, Y.G. Recycled oceanic crust in the source of 90–40 Ma basalts in North and Northeast China: Evidence, provenance and significance. *Geochim. Cosmochim. Acta* **2014**, *143*, 49–67. [[CrossRef](#)]
47. Sun, J.X.; Li, N.; Zhang, W.Q. Petrogenesis and characteristics of the mantle source for the Quaternary Datong basalt: Research on the major, trace elements and Sr–Nd–Pb–Hf isotopes. *Acta Petrol. Sin.* **2020**, *36*, 3331–3345.
48. Liu, F.; Cao, F.; Zhang, Z.X.; Li, Q. Chronology and geochemistry of the granite near the Keketuohai No3 pegmatite in Xinjiang. *Acta Petrol. Sin.* **2014**, *30*, 1–15.
49. Li, J.K.; Liu, X.F.; Wang, D.H. The metallogenetic regularity of lithium deposit in China. *Acta Geol. Sin.* **2014**, *88*, 2269–2283.
50. Middlemost, E.A.K. Naming Materials in the Magma/Igneous Rock System. *Earth-Sci. Rev.* **1994**, *37*, 215–244. [[CrossRef](#)]
51. Yu, H.L.; Yan, C.D.; Yu, F.Q.; Wang, D.F. Geochemical characteristics and tectonic environment of Eocene basalts of the Jiangling hollow. *Geol. Rev.* **1996**, *42*, 44–51.
52. Winchester, J.A.; Floyd, P.A. Geochemical discrimination of different magma series and their differentiation products using immobile elements. *Chem. Geol.* **1997**, *20*, 325–343. [[CrossRef](#)]
53. Guan, D.F. Geological conditions for the formation of oil and gas in the second subsidence zone of the New Cathaysia Series. *J. Daqing Petrol. Inst.* **1997**, *2*, 7–21.
54. Xu, Y.G.; Fan, Q.C. Cenozoic Volcanism in Eastern China: Review and Perspectives. *Bull. Mineral. Petrol. Geochem.* **2015**, *34*, 682–689.
55. Lin, W.; Wang, Q.C. Late Mesozoic extensional tectonics in the North China block: A crustal response to subcontinental mantle removal? *Bull. Soc. Geol. Fr.* **2006**, *117*, 287–297. [[CrossRef](#)]
56. Zhai, M.; Fan, Q.; Zhang, H.; Sui, J.; Shao, J.A. Lower crustal processes leading to Mesozoic lithospheric thinning beneath eastern North China: Underplating, replacement and delamination. *Lithos* **2007**, *96*, 36–54. [[CrossRef](#)]
57. Mao, J.W.; Xie, G.Q.; Li, X.F.; Zhang, Z.H.; Wang, Y.T.; Wang, Z.L.; Zhao, C.S.; Yang, F.Q.; Li, H.M. Geodynamic process and metallogeny: History and present research trend, with a special discussion on continental accretion and related metallogeny throughout geological history in South China. *Miner. Depos.* **2005**, *24*, 193–205.
58. Wu, L.L.; Mei, L.F.; Paton, D.A. Late Cretaceous–Cenozoic intraplate extension and tectonic transitions in eastern China: Implications for intraplate geodynamic origin. *Mar. Petrol. Geol.* **2020**, *117*, 104379. [[CrossRef](#)]
59. Yang, C.Q.; Chen, K.Q.; Chen, Z.Q.; Zhan, H.J. Constituent evolution and exploration potential in Jiangling depression. *Nat. Gas Ind.* **2003**, *23*, 51–54.
60. Xu, Y.G.; Ma, J.L.; Frey, F.A.; Feigenson, M.D.; Liu, J.F. Role of lithosphere interaction in the genesis of Quaternary alkali and tholeiitic basalts from Datong, western North China Craton. *Chem. Geol.* **2005**, *224*, 247–271. [[CrossRef](#)]
61. Chen, Y.; Zhang, Y.X.; Graham, D.; Su, S.; Deng, J. Geochemistry of Cenozoic basalts and mantle xenoliths in Northeast China. *Lithos* **2007**, *96*, 108–126. [[CrossRef](#)]
62. Palmer, M.R. Boron-isotope systematics of Halmahera arc (Indonesia) lavas: Evidence for involvement of the subducted slab. *Geology* **1991**, *19*, 215–217. [[CrossRef](#)]